

Università degli studi di Modena e Reggio Emilia

DIPARTIMENTO DI INGEGNERIA “ENZO FERRARI”

Corso di Laurea Magistrale in Ingegneria Meccanica

**Modelling and energy assessment
of a switched inertance hydraulic
system for pitch control**

Relatore:

Dott. Ing. Barbara Zardin

Candidato:

Alessio Galloni

Correlatore:

Prof. Victor Juliano De Negri

Anno Accademico 2013-2014

SOMMARIO

Questa tesi magistrale presenta uno studio teorico-sperimentale di un sistema di attuazione idraulico per la regolazione dell'angolo del passo di pale eoliche. L'energia eolica è oggi una delle più promettenti nuove forme di energia; ha visto negli ultimi anni una forte crescita in merito allo sviluppo in tutte le aree tecnologiche riguardanti la progettazione e costruzione di turbine eoliche. Una delle più grandi problematiche al momento è quella di aumentare l'efficienza del processo di prelievo di energia del vento. La regolazione dell'angolo del passo, applicato nelle turbine ad asse orizzontale, non solo permette di ottimizzare la raccolta di energia, ma riduce pure i carichi dinamici della struttura delle turbine e mantiene la potenza generata dentro standard stabiliti. In questo documento un modello analitico di un innovativo sistema idraulico per la regolazione dell'angolo del passo è proposto e validato da simulazioni ed esperimenti. Il sistema sfrutta la switching technology dell'idraulica digitale, utilizzando una valvola a rapida commutazione e una linea di trasmissione per alimentare un attuatore idraulico; ogni componente è descritto e il modello include gli effetti transitori della rapida commutazione, la non-linearità e le perdite della valvola. Inoltre, un confronto con le prestazioni di un sistema tipicamente utilizzato nell'industria eolica per la regolazione dell'angolo del passo è presentata. Scopo di questo studio, è quello di mostrare i vantaggi del nuovo sistema proposto per l'applicazione in termini di efficienza e risparmio energetico. Pretende inoltre di aggiungersi alle pubblicazioni attualmente presenti per lo studio di sistemi di controllo per la regolazione dell'angolo del passo di turbine eoliche, fornendo un efficace modello per comprendere, analizzare ed ottimizzare le caratteristiche e prestazioni del sistema.

Keywords: sistemi per il controllo del passo, sistemi idraulici, idraulica digitale, sistemi idraulici a rapida commutazione, turbine eoliche

ABSTRACT

This master's thesis reports on theoretical and experimental investigations of a switched inertance hydraulic system, which is designed for the blade pitch control of a wind turbine. Wind power is nowadays one of the most promising new energy resource; it has shown, in the last years, a considerable growth in development of all the technological areas involving design and construction of wind turbines. One of the biggest current challenges is to increase the efficiency of the wind capture. The blade pitch control, applied in the horizontal axis wind turbine, permits not only to optimize the energy capture, but also to reduce the dynamic loads in the turbine structure, and to maintain the quality of the generated power according to the standard requirements.

In this context, an analytical model of an innovative hydraulic system for pitch control is proposed and validated by simulation and experiments. The system consists of a switching valve, a transmission line and a hydraulic linear actuator; every component is described and the model includes the effects of switching transition, non-linearity and leakage of the valve. In addition, a comparison with a hydraulic system conventionally applied in the wind industry for the blade pitch control is presented. The objective of this study is to show the advantages of the new designed system for the application, in term of more efficiency and energy saving. It also pretends to contribute to the area of pitch control systems for wind turbines, providing a very effective model for understanding, analysing and optimising the characteristics and performance of the system.

Keywords: pitch control systems, hydraulic systems, digital hydraulics, switched inertance hydraulic systems, wind turbine

ACKNOWLEDGES

I would like to express my gratitude to everyone who has contributed to make this thesis a reality.

In particular I am grateful to my supervisor professor Victor Juliano De Negri, for his support, guidance and valuable advices. He introduced me to the hydraulic community and welcomed me as one of his students, I cannot thank him enough for this.

Particular huge thanks go out to my friends at LASHIP, who make me feel home with their friendship and help me out during difficult moments. Among them, Marcos deserves a special mention for his perseverance on facing the adversities which the test bench thrown to us. Without him this dissertation would not have been possible.

Special thanks to my family, for their love and support along my whole life. I will always be grateful to my mother for her presence and assistance.

I would like to acknowledge my old friends who looked after me even though the long distance and an ocean or two between us. I feel fortunate to have them.

To conclude, I owe my gratitude to my supervisor Ing. Barbara Zardin for all the support I received during the writing of this thesis. She has challenged and enriched my ideas under a wise and helpful guidance improving this way the developing of the thesis.

Contents

Notation	vii
1 Introduction	2
1.1 Background	2
1.2 Objectives	2
1.3 Grounds	3
1.4 Outline	4
2 Wind Energy	5
2.1 Global Wind Power	5
2.2 Aerodynamics of wind rotors and classification	7
2.3 Horizontal Axis Wind Turbines	9
2.4 Rotor Blade Pitching	11
2.4.1 Hydraulic system for pitch control	16
3 Digital Fluid Power	18
3.1 Definition and branches of Digital Fluid Power	18
3.2 Parallel Connection Technology	19
3.3 Switching Systems	21
3.3.1 The switched inertance system	22
3.4 A comparison between digital fluid power and traditional systems	24
3.5 The digital hydraulic system for pitch control	25
4 Modelling of the hydraulic system	27
4.1 Hydraulic Cylinder	27
4.1.1 Equation of motion	27
4.1.2 Friction Force	29

4.1.3	Continuity Equation	30
4.2	Proportional Directional Valve	33
4.2.1	Proportional Valve	34
4.2.2	Switching Valve	38
4.3	Inertance Tube	40
4.4	Accumulator	42
4.5	Control Unit	48
5	Theoretical and Experimental Results	51
5.1	Test Bench	51
5.2	Simulations	56
5.3	Results	57
5.4	Energy Assessment	64
6	Conclusions	67
	Appendix A Transmission Line Method (TLM)	74
	Appendix B Component Details	78
	Appendix C Matlab Code	80

List of Figures

2.1	Map of the Global Mean Speed at 80m [1]	6
2.2	Global Installed Wind Capacity [2]	6
2.3	The energy extracting stream-tube of a wind turbine [3]	8
2.4	Overview of the different types of wind turbines. [4]	9
2.5	HAWT rotor configurations [5]	10
2.6	Details of a typical horizontal axis wind turbine [6]	11
2.7	Power input of the WKA-60 rotor for various blade pitch angles and at a fixed rotor speed [6]	12
2.8	Influence of blade pitch control on the smoothing of the electric power output [6]	13
2.9	Pitch linkage system used in conjunction with a single hydraulic ac- tuator [3]	14
2.10	Blade linkage system using separate hydraulic actuators for each blade [3]	15
2.11	Partial blade pitching in Howden HWP-1000 turbine rotor [6]	16
2.12	A Rexroth application using hydraulic system for regulating the pitch angle of a three blade wind turbine [7]	17
3.1	Parallel connected system (a), the simplified drawing symbol of the parallel connected system (b) [8]	19
3.2	Relative DFCU output for 3, 5 and 7 valves with binary and PNM coding [8]	20
3.3	the implementation of distributed four-way valve by DFCU [8]	21
3.4	Switching controlled valve by PWM [8]	21
3.5	Pressure Booster: a) Hydraulic circuit; b) Electrical circuit	22
3.6	Flow Booster: a) Hydraulic circuit; b) Electrical circuit	23

3.7	Real inertance tube	24
3.8	Hydraulic circuit diagram	25
4.1	Forces acting on the cylinder	28
4.2	Simulink diagram of the equation of motion	29
4.3	Diagram of the Gomes friction model [9]	30
4.4	Continuity equation for the double-acting hydraulic cylinder	31
4.5	Simulink diagram of the continuity equation for the cylinder	33
4.6	Intern of a three-way valve, [10]	34
4.7	Simulink diagram of the proportional valve	37
4.8	Simulink diagram of the switching valve	40
4.9	Supply pressure and example of flow rate with an ideal instantaneous switching transition [11]	41
4.10	Pressure diagrams with different dampeners [12]	42
4.11	Basic types of hydraulic accumulators [13]	43
4.12	Operations of the diaphragm accumulator [13]	44
4.13	Directional component for the accumulator	47
4.14	Simulink diagram of the accumulator	48
4.15	Diagram of a PID controller	49
4.16	Scheme of the applied system control	50
4.17	Simulink diagram of the SIHS	50
5.1	Application of the HIL [14]	52
5.2	Hydraulic/mechanical system of the test bench	53
5.3	a) Scheme of the test bench b) Geometrical parameters [14]	54
5.4	Test Bench Diagram (adapted from [14])	56
5.5	Responses of the system to angular steps using a force $F_c = 10$ kN	57
5.6	Responses of the system to angular steps using a force $F_c = -10$ kN	58
5.7	Responses of the system comparing different PI controllers	59
5.8	Flow rate through the valve	60
5.9	Control signals of the valve	60
5.10	Flow rate through the valve	60
5.11	Control signals of the valve	60

5.12	Enlargement of the flow rate through the valve	61
5.13	Enlargement of the control signals of the valve	61
5.14	Pressures with $F_c = 10\text{kN}$	61
5.15	Pressures with $F_c = -10\text{kN}$	61
5.16	Enlargement of the pressures with $F_c = 10\text{kN}$	62
5.17	Enlargement of the pressures with $F_c = -10\text{kN}$	62
5.18	Simulated responses of the system comparing different forces	62
5.19	Experimental responses of the system comparing different forces	63
5.20	Responses using critical forces	64
5.21	Diagram of the power assessment	64
5.22	Simulink of the proportional system	66
A.1	Pipeline	75
A.2	Block diagram for the TLM [15]	76

Notation

A_A	area of chamber A of the cylinder	$[m^2]$
A_B	area of chamber B of the cylinder	$[m^2]$
A_s	rotor swept area	$[m^2]$
$A_{3,4}$	area of the orifices of the valve	$[m^2]$
B	damping coefficient	$[\text{kg/s}]$
cd	coefficient of the orifices of the valve	$[\sqrt{m^3/kg}]$
C_p	power coefficient	
C_{in}	internal leakage constant	$[m^3/(s \cdot Pa)]$
$\frac{dV}{dt}$	rate of volume change	$[m^3/s]$
$\frac{dV_A}{dt}$	rate of volume change within chamber A	$[m^3/s]$
$\frac{dV_B}{dt}$	rate of volume change within chamber B	$[m^3/s]$
$\frac{dV_g}{dt}, \dot{V}_g$	rate of change of gas volume	$[m^3/s]$
$\frac{dV_f}{dt}, \dot{V}_f$	rate of change of fluid volume in the accumulator	$[m^3/s]$
$\frac{dp}{dt}$	rate of pressure change	$[\text{Pa/s}]$
$\frac{dp_A}{dt}$	rate of pressure change within chamber A	$[\text{Pa/s}]$
$\frac{dp_B}{dt}$	rate of pressure change within chamber B	$[\text{Pa/s}]$
$\frac{dp_g}{dt}, \dot{p}_g$	rate of change of gas pressure	$[\text{Pa/s}]$
$\frac{dx}{dt}$	velocity of the piston	$[\text{m/s}]$
$\frac{d^2x}{dt^2}$	acceleration of the piston	$[m/s^2]$
e(t)	signal error	$[^\circ]$
f	frequency of the signal control Uc	$[\text{Hz}]$
F_L	loading force	$[\text{N}]$
F_{fr}	friction force	$[\text{N}]$
F_{sp}, F_{sn}	static friction forces	$[\text{N}]$
F_p	hydraulic force	$[\text{N}]$

F_c	force acting on the control system	[N]
\vec{F}_c	vector of the force F_c	[N]
K_x	spring coefficient	[kg/s ²]
K_v	flow coefficient	[m ³ /(s · √Pa)]
$K_{v_{in}}$	leakage flow coefficient	[m ³ /(s · √Pa)]
K_p	proportional constant PID	
K_i	integral constant PID	
K_d	derivative constant PID	
$L_{p,f}$	distances between the rotation axis and the cylinder joints	[m]
L_c	distance between the control cylinder and the head of the piston rod	[m]
L_{pF}	distance between the joints of the cylinders	[m]
M_t	total mass of the system	[kg]
M_L	mass of the load	[kg]
M_f	mass of the fluid	[kg]
M_{cyl}	mass of the cylinder	[kg]
M_p	maximum peak of the overshoot	[%]
n	index, exponent	
P	output power of a wind turbine	[W]
p_A	pressure chamber A of the cylinder	[Pa]
p_B	pressure chamber B of the cylinder	[Pa]
p_{HP}	pressure at high pressure port	[Pa]
P_{HP}	instant power at high pressure port	[W]
p_{LP}	pressure at low pressure port	[Pa]
P_{LP}	instant power at high pressure port	[W]
P_B	instant power at chamber B	[W]
P_{mecc}	useful instant power	[W]
P_{LOSS}	lost instant power	[W]
P_{Hyd}	instant power introduced by the power unit	[W]
p_0	accumulator charging pressure	[Pa] (abs)
p_1	maximum system pressure	[Pa] (abs)

p_2	minimum system pressure	[Pa] (abs)
p_g	pressure of the gas at instant t	[Pa]
P^{CC}	moment arm of the control cylinder	[m]
P^{CF}	moment arm of the force cylinder	[m]
q_{Vn}	nominal flow rate of the valve	[l/min]
q_{Vp}	leakage flow rate of the valve	[l/min]
$q(t)$	flow rate in time domain	[l/min]
q_m	mean delivery flow rate	[l/min]
Q_n	amplitude of the harmonic n	[l/min]
Q_1	flow in	[l/min]
Q_2	flow out	[l/min]
q_{VA}	flow in chamber A	[l/min]
q_{VB}	flow out chamber B	[l/min]
q_{Vin}	internal leakage of the cylinder	[l/min]
q_{VHP}	flow rate at high pressure port	[l/min]
q_{VLP}	flow rate at low pressure port	[l/min]
$r_{p,f}$	distance of the head of the piston rods and the rotational axis of the blade	[m]
v_w	velocity of the wind	[m/s]
\vec{v}	vector of the velocity of the piston	[m/s]
V	control volume	[m ³]
V_A	volume of chamber A of the cylinder	[m ³]
V_B	volume of chamber B of the cylinder	[m ³]
V_{A0}	volume of chamber A of the cylinder when x = 0	[m ³]
V_{B0}	volume of chamber B of the cylinder when x =0	[m ³]
V_f	volume of the fluid in the accumulator	[m ³]
V_g	volume of gas in the accumulator	[m ³]
V_0	is the accumulator size or capacity, volume of charging gas at pressure p_0	[m ³]
V_1	is the volume of gas at pressure p_1	[m ³]
V_2	is the volume of gas at pressure p_2	[m ³]
$y_{sp}(t)$	input set point	[°]

$y(t)$	output signal	[°]
$u(t)$	error after the PID	[°]
U_c	signal control	[V]
U_n	nominal control signal	[V]
T	period of U_c	[s]
t_r	rise time	[s]
t_s	settling time	[s]
x	motion of the cylinder	[m]
x^{VP}	motion of the spool of the valve	[m]
$\dot{x}_{0p}\dot{x}_{0n}$	“stick” velocity (positive and negative sense)	[m/s]
$\dot{x}_{limp}\dot{x}_{limn}$	friction velocity limits (positive and negative sense)	[m/s]
$X^{VP}(s)$	Laplace transform of x^{VP}	
$U_c(s)$	Laplace transform of U_c	
ρ_a	density of air	[kg/m ³]
λ	duty cycle of the signal control U_c	
β	angle of attack of the blade	[°]
β_e	effective Bulk Modulus	[Pa]
$\tau_{p,F}$	angle between $r_F - L_F$ and $r_p - L_p$ respectively	[°]
$\theta_{p,F}$	angle between the cylinders and L_p o L_F	[°]
γ	constant for adiabatic process	
Δ_{pn}	pressure which delivers q_{V_n}	[Pa]
Δ_{ps}	pressure which delivers q_{V_p}	[Pa]
ω_n	natural frequency of the valve	[rad/s]
ξ	damping ratio	

1

Introduction

1.1 Background

In the last years, wind power capacity has expanded rapidly and wind energy production was around 4% of total worldwide electricity usage in June 2014 [16]. Great efforts have been made by the research for reaching those results. In particular, increasing the power of wind generators is a tough and ambitious task which involves improvements in all the technological areas related to the construction and design of wind turbines. However, one of the most valuable aspect for enhancing the efficiency is the power control; it can be realized with different approaches, according to the wind turbine typology, but the most common method is to regulate the blade pitch angle. That solution not only permits to set the output power within specified standards, but also increases the efficacy of the wind energy capture and reduces the dynamic loads which act on the wind turbine structure.

1.2 Objectives

Scope of this work is to introduce the reader to wind power and the systems currently applied on wind turbines for regulating the blade pitch and presenting a new system which take advantage of the digital hydraulics for improving the efficiency and energy savings.

In order to carry out that purpose, specific elements need to be met:

- an introduction on worldwide wind power capacity and the reasons which lead

to a growing interest on investing in wind turbines, followed by a description and comparison of the different pitch control systems in order to comprehend the present possibilities

- an overview over digital hydraulics necessary to understand the different techniques and in particular the switching technology which is largely used in this work
- a description and design of the new switched inertance hydraulic system, along with its analytical model
- the implementation of the model proposed with the model-based software MATLAB/*Simulink* able to perform dynamic simulations
- validation and confrontation of the data achieved by the simulations with experimental results obtained by tests conducted on an experimental test bench which reproduces the hydraulic system
- evaluation of energy savings and efficiency of the new hydraulic system
- evidence of the advantages found comparing the data with the results achieved by simulations and experiments using a conventional hydraulic system for pitch control typically applied on commercial wind turbines.

1.3 Grounds

Wind energy as an alternative to fossil fuels, is plentiful, renewable, widely distributed, clean, produces no greenhouse gas emissions during operation and uses little land [17]. However, the energy industry is a competitive environment where the renewable resources have to evince their advantages in order to stimulate the research and their usage. For this reason, continuous improvements towards more efficiency and power need to occur.

In this setting, the present work aims to offer a new solution able to amend the present systems used for blade pitching proposing a more efficient device.

1.4 Outline

This master's thesis is organized as follow:

in chapter 2, an overview on wind power and the exiting typologies of wind turbines are presented. Moreover, the actuation systems for regulating the blade pitch of horizontal axis wind turbines are introduced.

Chapter 3 describes the state of art of digital fluid power. Several technologies are matter of study these days, but the focus of this section increases on the switching technology. In addition the new hydraulic system for pitch control is proposed.

The system described in chapter 3 is now studied in chapter 4, where analytical models are presented beside their implementation in the software MATLAB/*Simulink*.

Chapter 5 introduces the experimental test bench and shows the trial results which are compared with the data obtained from the dynamic simulations. In addition, it presents the results achieved by an energy assessment in order to evince efficiency and energy saving.

Finally, chapter 6 evidences the energy efficiency and the advantages of the new proposed system and suggests possible future developments.

2

Wind Energy

In this chapter the state of art of wind power, focusing on the energy conversion systems will be introduced. Later on, an overview of the different methods used in order to control blade pitch angle are presented.

2.1 Global Wind Power

It is widely accepted in scientific community that there is enough power in the Earth's winds to be a primary source of near-zero-emission electric power as the global economy continues to grow through the twenty-first century [18].

Wind potential studies carried out in the last 10 years have resulted in phenomenal outcomes regard to global wind energy. Marvel et al. [18] have estimated a global wind energy potential of 400 TW, which is many times higher than the actual electricity generation capacity in the world (nearly 6250 GW [19]). Similarly, an assessment conducted by Archer et al. [20] projects a worldwide potential of 72000 GW, using 1.5 MW wind turbines at 80m hub height. Xi et al. [21] have concluded that a network of land-based 2.5 MW turbines restricted to non-forested, ice-free, non-urban areas operating at as little as 20% of their rated capacity could supply >40 times current worldwide consumption of electricity, >5 times total global use of energy in all forms.

In 2014 the energy efficiency company 3TIER mapped the global wind potential distribution, providing the mean wind speed evaluated at 80m high as illustrated in figure 2.1.

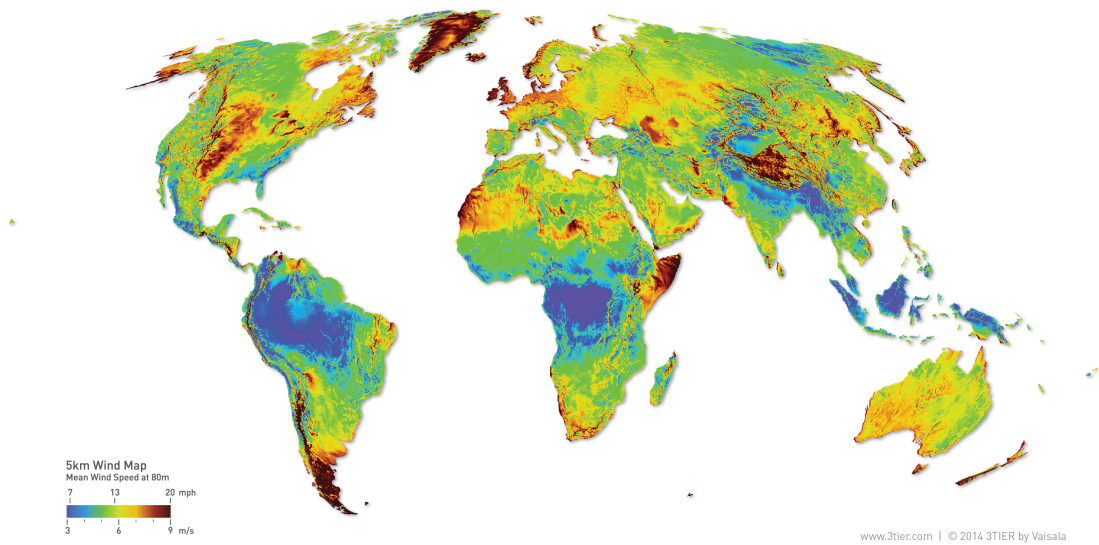


Figure 2.1: Map of the Global Mean Speed at 80m [1]

We see in the review of the scientific assessments presented that there is indeed enough energy in the winds that blow on the surface of this planet to meet all energy requirements. It is then reasonable to conclude that looking at global electricity requirements and even growth in electricity over the next few decades, it is possible to meet all electricity requirements with technologies and options that are a combination of wind, solar, hydro and biomass and storage technologies and devices. Technically, it is possible to phase out nuclear and fossil fuel based generating stations [16].

Based on these observations, plenty of companies and countries have invested in the wind energy along the last few years establishing a trend that is going to rise in the next future (see figure 2.2).

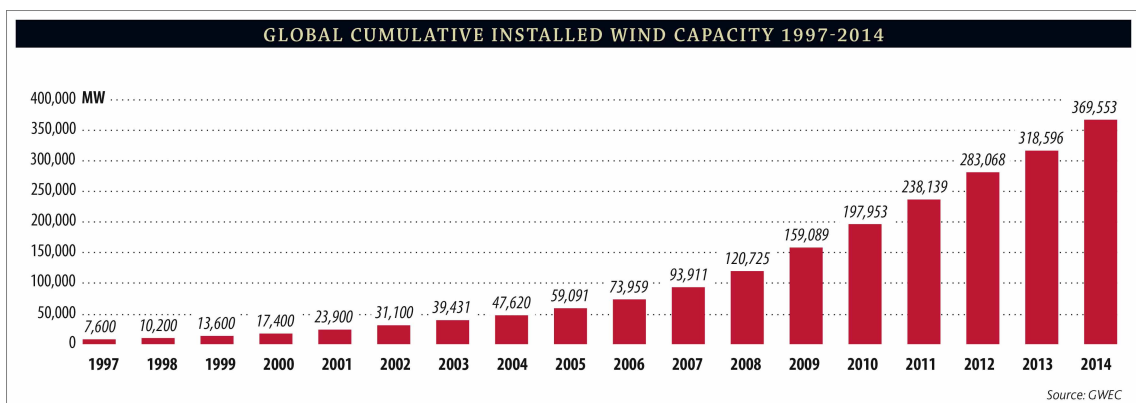


Figure 2.2: Global Installed Wind Capacity [2]

2.2 Aerodynamics of wind rotors and classification

The output power (P) of a wind turbine is given by the well-known expression:

$$P = \frac{1}{2}C_p\rho_a A_s v_w^2$$

where ρ_a is the density of air ($1,204 \text{ kg}/\text{m}^3$ at 20C and 101.325 kPa), C_p is the power coefficient, A_s is the rotor swept area, and v_w is the wind speed.

A wind turbine is a device which extracts kinetic energy from the wind. Although kinetic energy is taken from the airflow, a sudden step change in velocity is neither possible nor desirable because of the enormous accelerations and forces this would require. Pressure energy can be extracted in a step-like manner and all wind turbines, whatever their design, operate in this way.

The presence of the turbine causes the approaching air, upstream, gradually to slow down such that when the air arrives at the rotor disc its velocity is already lower than the free-stream wind speed. The stream-tube expands as a result of the slowing down and, because no work has yet been done on, or by, the air its static pressure rises to absorb the decrease in kinetic energy.

As the air passes through the rotor disc, by design, there is a drop in static pressure such that, on leaving, the air is below the atmospheric pressure level. The air then proceeds downstream with reduced speed and static pressure. Eventually, far downstream, the static pressure must return to the atmospheric level for equilibrium to be achieved. The rise in static pressure is at the expense of the kinetic energy and so causes a further slowing down of the wind. Thus, between the far upstream and far downstream conditions, no change in static pressure exists but there is a reduction in kinetic energy [3].

In figure 2.3 can be seen the stream-tube airflow of a wind turbine.

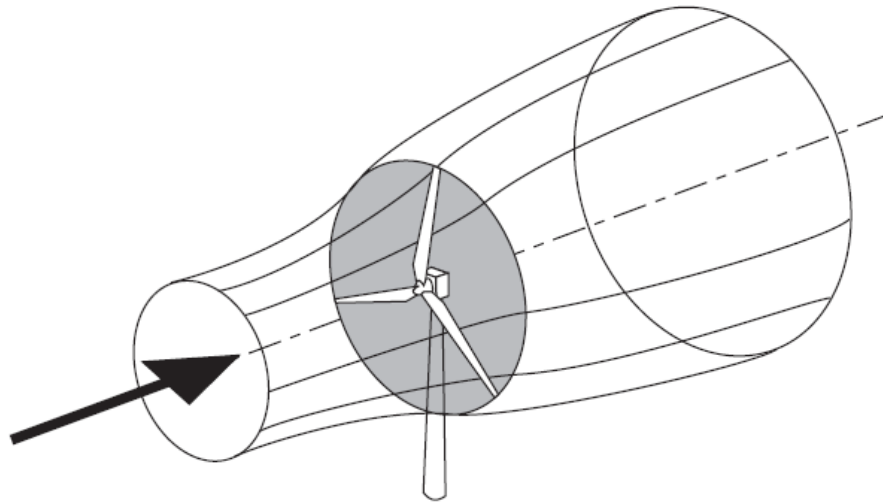


Figure 2.3: The energy extracting stream-tube of a wind turbine [3]

Today there are various types of wind turbines in operation, (see figure 2.4). In particular, the most common device is the horizontal axis wind turbine (HAWT). This turbine consists of only a few aerodynamically optimised rotor blades, which for the purpose of regulation usually can be tumbled about their long axis (Pitch-regulation). These turbines can deliver power ranging from 10 kW to some MW.

The efficiency of this type of turbine is very high. Therefore, it is solely used for electricity generation which needs high-speed electric motors to keep the gear transmission and the generator small and cheap.

Another conventional but older type of horizontal-axis rotor, is the multi-blade wind turbine. It was first built about one hundred years ago. Such wind mills have a high starting torque which makes them suitable for driving mechanical water pumps. The number of rotations is low, and the blades are made from simple sheets with an easy geometry.

A third type of turbines is characterized by a vertical-axis construction (VAWT). They are noisier than horizontal-axis turbines and another disadvantage is that wind velocity increases significantly with height, making horizontal-axis wheels on towers more economical. Nevertheless, there are some companies which produce DARRIEUS type VAWTs in the very low power range of a few kilowatts for decentralised electricity supply in areas without electrical grids, e.g., in rural areas of developing countries [4].

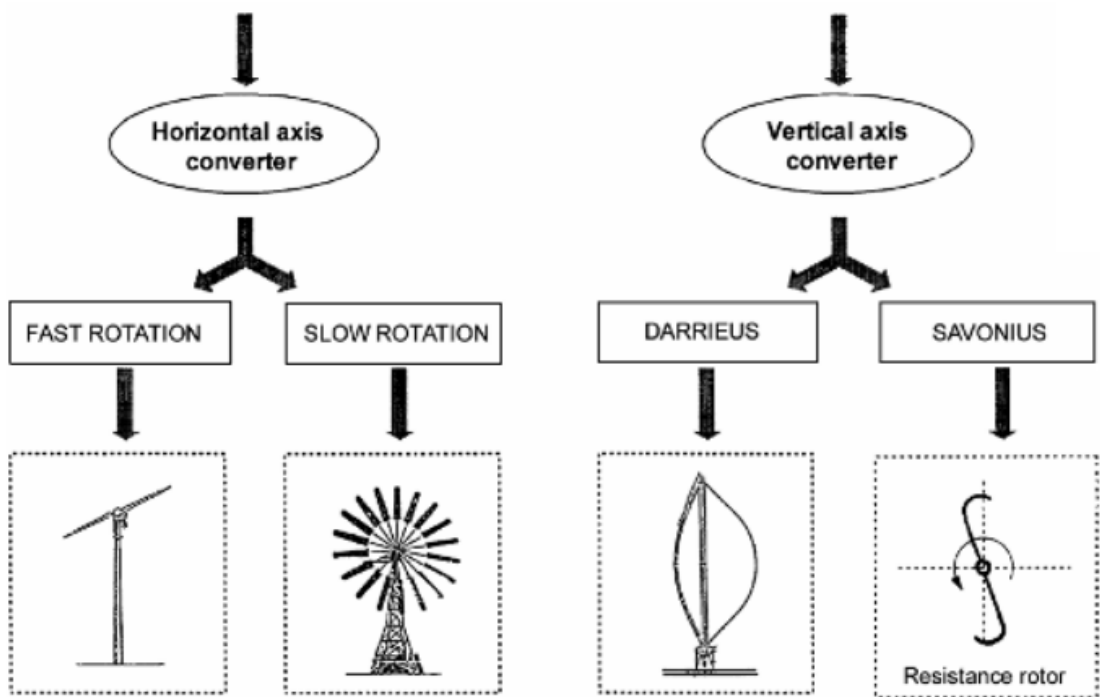


Figure 2.4: Overview of the different types of wind turbines. [4]

The focus of this paper is a tool which is applied on horizontal axis wind turbines. For this reason, henceforth the HAWT is the only configuration discussed and it has to be considered as synonym of wind turbine along the study. The next section discusses that design in details.

2.3 Horizontal Axis Wind Turbines

HAWTs are usually classified according to the rotor orientation (upwind or downwind of the tower), hub design (rigid or teetering), rotor control (pitch vs. stall), number of blades (usually two or three blades), and how they are aligned with the wind (free yaw or active yaw) [5]. Figure 2.5 shows the upwind and downwind configurations.

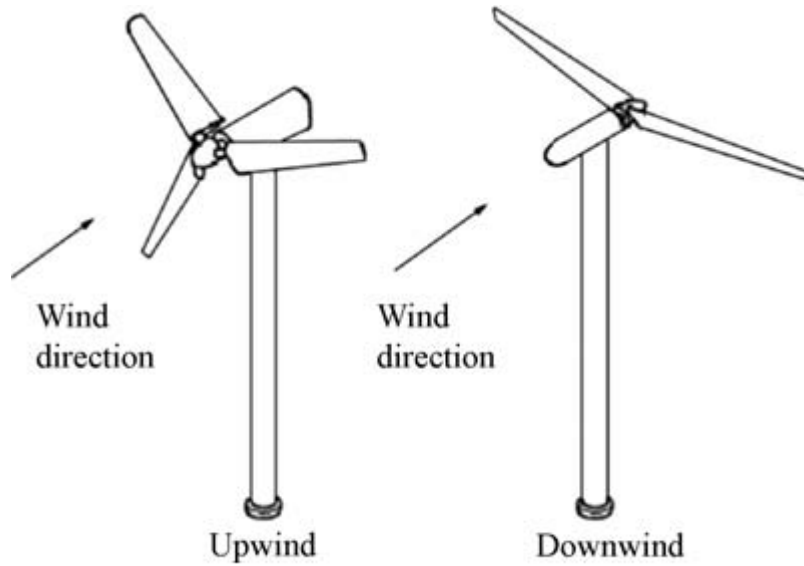


Figure 2.5: HAWT rotor configurations [5]

According to Hau [6], the undisputed superiority of the HAWT design is largely based on the following characteristics:

- in propeller designs, rotor speed and power output can be controlled by pitching the rotor blades about their longitudinal axis (blade pitch control). In addition, rotor blade pitching is the most effective protection against over-speed and extreme wind speeds, especially in large wind turbines.
- the rotor blade shape can be aerodynamically optimised and it has been proven that it will achieve its highest efficiency when aerodynamic lift is exploited to a maximum degree.
- not least, the technological lead in the development of propeller design is a decisive factor.

Together, these advantages are the reason why almost all wind turbines for generating electricity built to date have horizontal-axis rotors.

The details of a typical HAWT are shown in figure 2.6. The main aspect of the classic design is the split shaft system, where the main shaft turns slowly with the rotor blades and the torque is transmitted through a gearbox to the high-speed secondary shaft that drives the few-pole pair generator.

The transmission of torque to the generator is shut off by means of a large disk brake on the main shaft. A mechanical system controls the pitch of the blades, so pitch control can also be used to stop the operation of the turbine in e.g. storm conditions. The pitch mechanism is driven by a hydraulic system, with oil as the popular medium. For constructions without a main brake, each blade has its pitch angle controlled by a small electric motor.

Wind speed and direction measuring instruments are located at the back of the hub head. A rack-and-pinion mechanism at the join of the hub and the tower, allows the hub to be rotated in to the wind direction, and out of it in storm conditions [6].

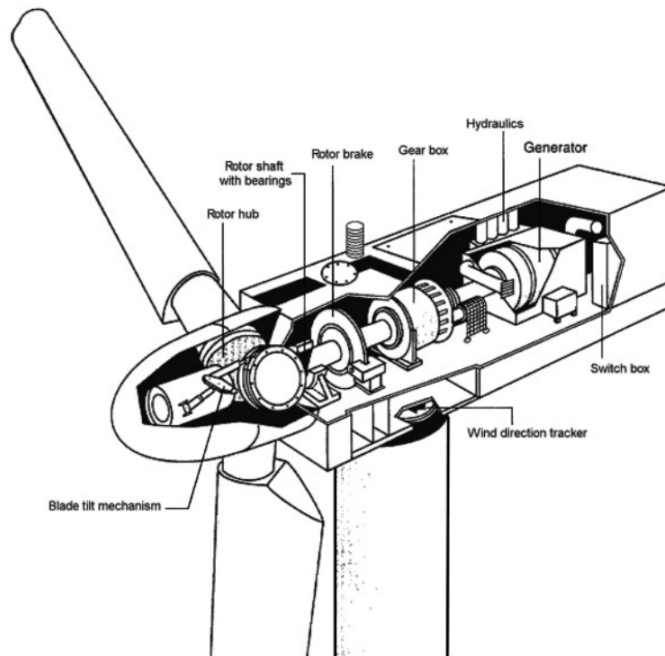


Figure 2.6: Details of a typical horizontal axis wind turbine [6]

2.4 Rotor Blade Pitching

At high wind speed, the power captured from the wind by the rotor far exceeds the limits set by the designed strength of the rotor structure [6]. This is especially true for large turbines as the strength limits of the components narrower with increasing turbine size. In addition, the power output of the rotor is limited by the maximum permissible power of the generator. Figure 2.7 shows to what extent the power input of the rotor increases when it is not subject to a control system.

Apart from limiting the power of the rotor, it is important to maintain the

rotor speed at a constant value or within certain limits. Speed control becomes indispensable when, for example the generator torque is suddenly lost. In such a case, rotor speed would increase extremely rapidly and would certainly lead to the destruction of the turbine unless countermeasures were taken immediately. The rotor of a wind turbine must, therefore, have an aerodynamically effective means for limiting its power and rotational speed [6].

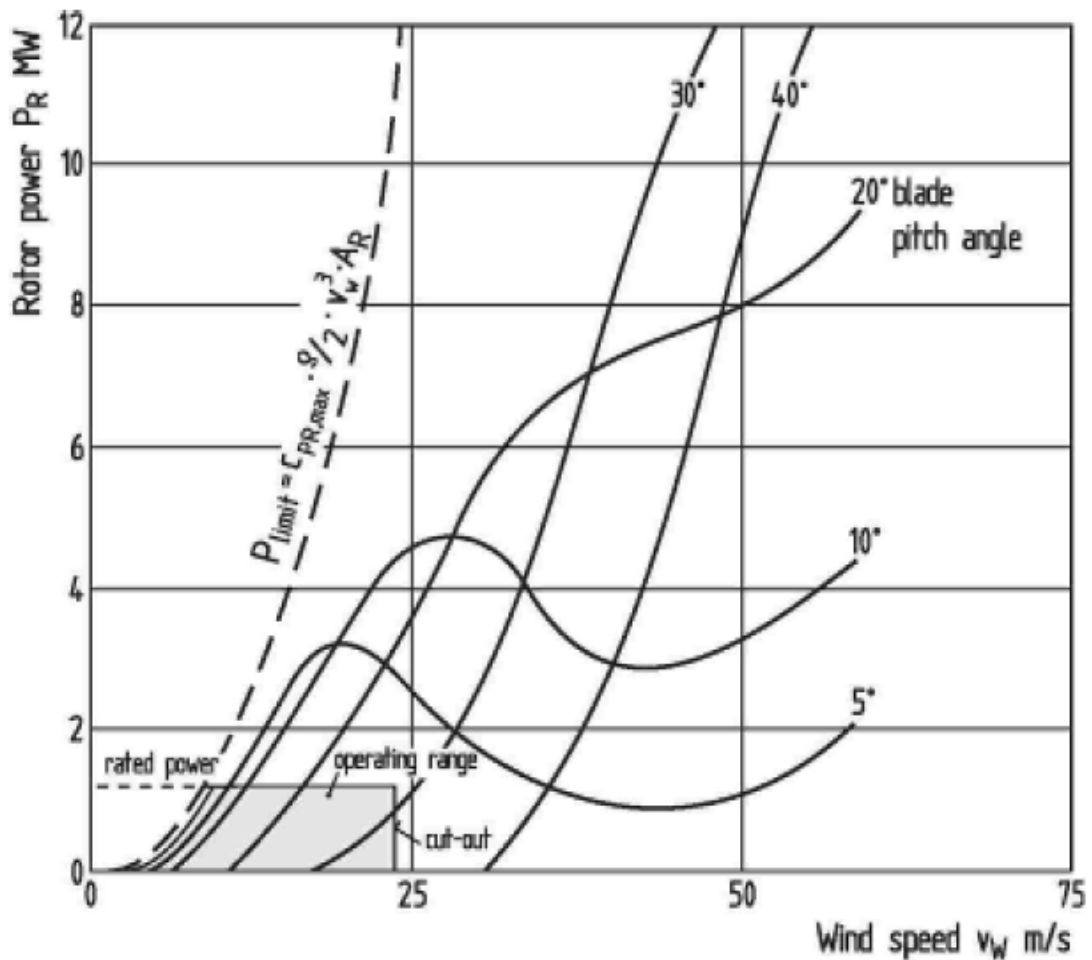


Figure 2.7: Power input of the WKA-60 rotor for various blade pitch angles and at a fixed rotor speed [6]

Basically, the driving aerodynamics forces can be reduced by influencing the aerodynamic angle of attack, by reducing the projected swept area of the rotor, or by changing the effective free-stream velocity at the rotor blades.

By far the most effective way of regulating the input power is influencing the aerodynamics angle of attack, by adjusting the rotor blade pitch angle. Several techniques exist in order to perform the above operation, both passive and active.

However the most convenient approach up to now, it has been the active blade pitch control.

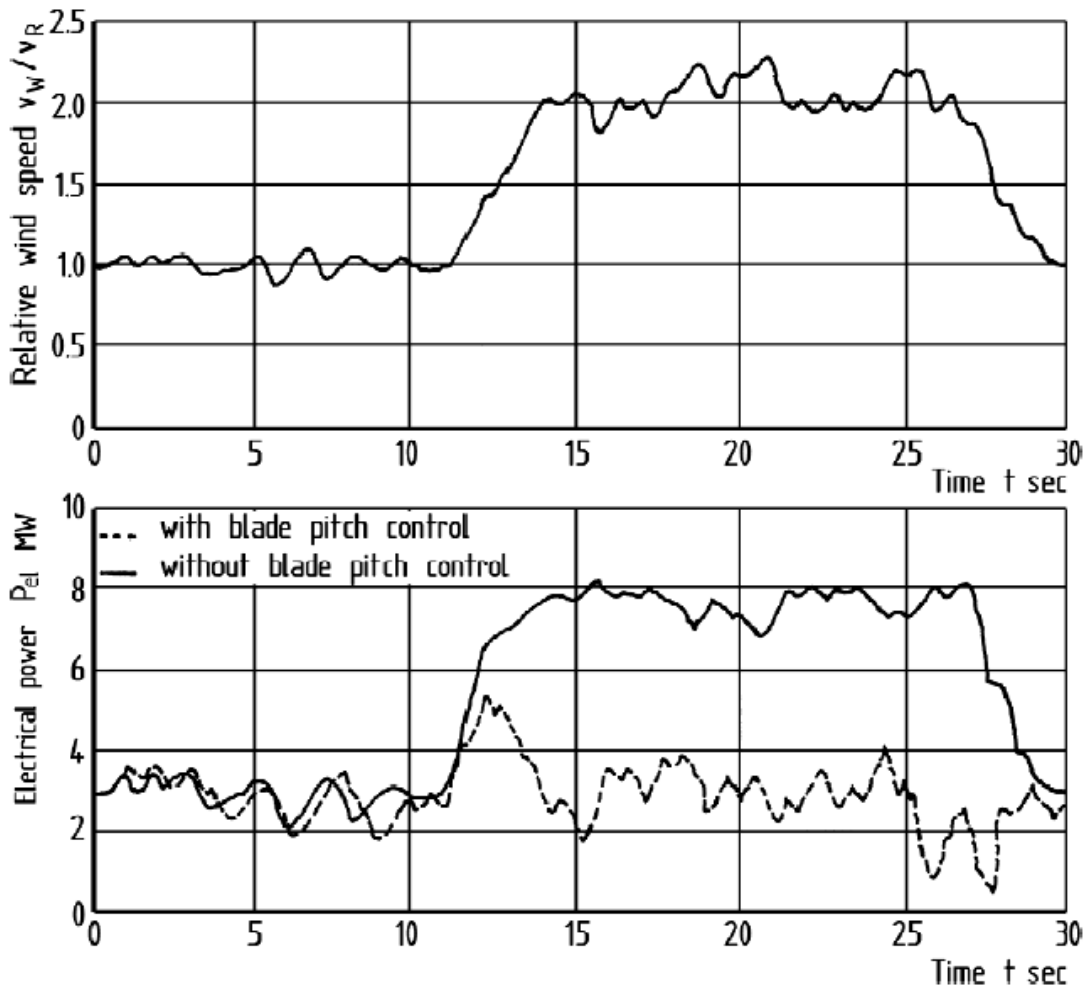


Figure 2.8: Influence of blade pitch control on the smoothing of the electric power output [6]

The main distinguishing feature of blade pitch systems is the type of actuators. The alternatives are hydraulic pitch actuators or electric motors. The newer turbines tend to install electric motors, but nevertheless, the hydraulic drives are still the most commons thanks to different advantages:

- fewer components with less overall installed size than in the case of electrical systems
- higher actuating force
- better dynamics, especially shorter response times for pitching actions and faster restart because no batteries have to be recharged

- no maintenance and service-life problems of electric batteries
- no wear problems in the pitching gears

Both electric and hydraulic drives are divided between those in which the blade has its own actuator and those in which a single actuator pitches all the blades. The first approach has the advantage that it provide several independent braking systems to control overspeed, and the disadvantage that it requires very precise control of pitch on each blade in order to avoid unacceptable pitch angle differences during normal operation. An advantage of the latter arrangement is that the pitch actuator, can be located in the nacelle, producing fore-aft motion of the pitch linkages in the hub by means of a rod passing down the middle of a hollow low-speed shaft (see figure 2.9) [3].

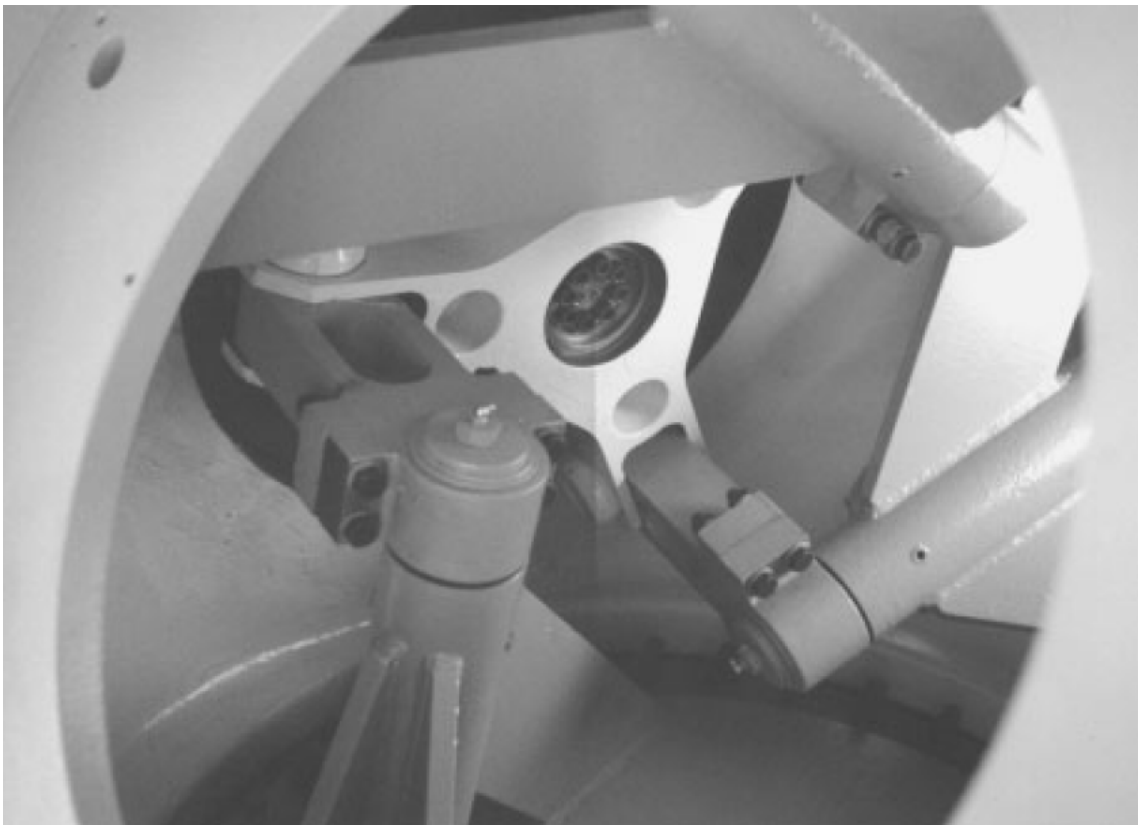


Figure 2.9: Pitch linkage system used in conjunction with a single hydraulic actuator [3]



Figure 2.10: Blade linkage system using separate hydraulic actuators for each blade [3]

Although full blade pitching is the option favoured by the overwhelming majority of manufactures, power control can still be fully effective even if only the outer 15 % of the blade is pitched (see figure 2.11). According to Burton et al. [3], the principal benefits are that the duty of the pitch actuators is significantly reduced, and that the inboard portion of the blade remains in stall, significantly reducing the blade load fluctuations. On the other hand partial blade pitch control has several disadvantages as follows:

- the introduction of extra weight near the tip
- the difficulty of physical accommodating the actuator within the blade profile
- the high bending moments to be carried by the tip-blade shaft
- the need to design the equipment for the high centrifugal loadings found at large radius
- the difficulty of access for maintenance

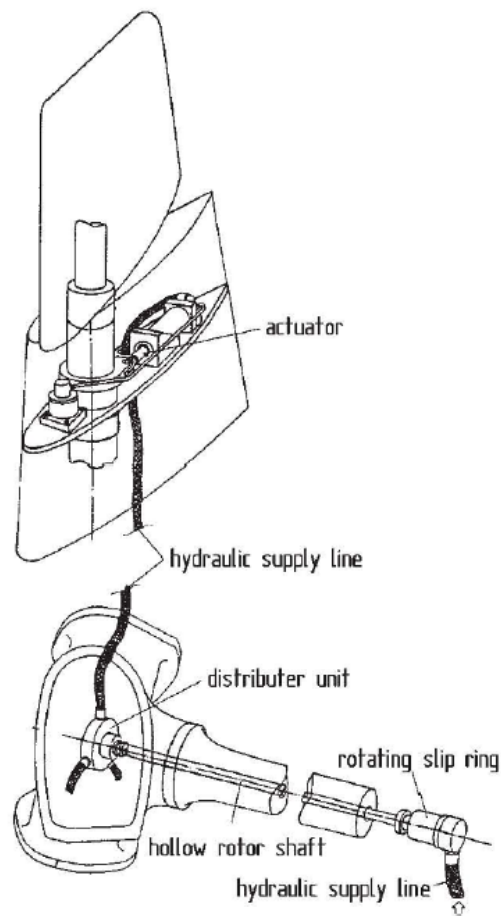


Figure 2.11: Partial blade pitching in Howden HWP-1000 turbine rotor [6]

From the above briefing of pitch actuation systems, it should be clear that the design of the hardware required for regulating the rotor blade pitch angle is a significant task. For this reason, the next section describes a typical system configuration using hydraulic actuators

2.4.1 Hydraulic system for pitch control

In order to regulate the pitch position of a wind turbine blade, a hydraulic system using mineral oil as fluid power is the most common solution, as seen in section 2.4.

The hydraulic system applied for that operation is theoretically simple, composed by a valve for regulating the flow required to a cylinder linked to a base which acts on a lever system able to rotate the blade around his axis (see figure 2.12). The matching valve/cylinder rotates around a fulcrum located on the blade which follows the blade movements and permits the adjustment of the cylinder position.

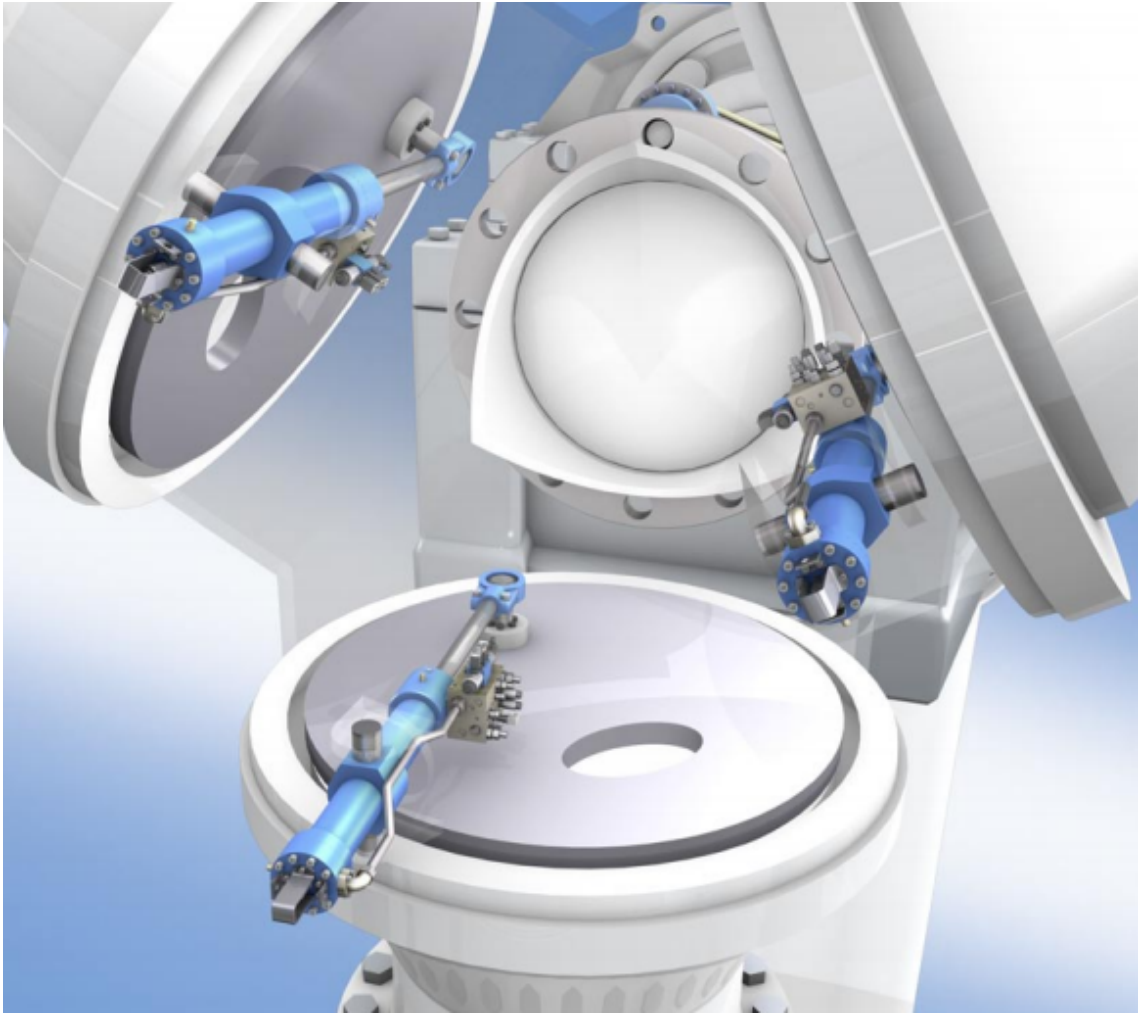


Figure 2.12: A Rexroth application using hydraulic system for regulating the pitch angle of a three blade wind turbine [7]

Typically commercial industries use a proportional hydraulic valve for implementing their systems. Nevertheless, the next chapter introduces a new hydraulic system which uses a switching valve and an inertance tube in order to improve the energy efficiency.

3

Digital Fluid Power

This chapter summarizes the present research results of digital fluid power and introduces different applications. In addition, the switched inertance hydraulic system object of this thesis is finally presented.

3.1 Definition and branches of Digital Fluid Power

According to Linjama [8], the term “Digital Fluid Power” is broad and not fully defined. However, the author suggests a definition of digital fluid power valid for both hydraulics and pneumatics: *“Digital Fluid Power means hydraulic and pneumatic systems having discrete valued component(s) actively controlling system output”*.

Two are the fundamental areas in which digital fluid power is divided: systems which use parallel connections and systems based on the switching technology. In the parallel connection, the system consists of parallel connected components which generate the overall output as combination of the single response of each component. As a result, the total output is characterized by a certain number of discrete values and no switching phenomena of the components is required for maintaining the output value. On the other hand, the switching technology uses a fast and continuous switching of single or a few components for reaching the desired output. Both the techniques found their use in different applications. However, in order to focus on the case of study only digital hydraulic valves are discussed next. Hydraulic circuit diagrams are given by using two-way on/off valves only because it is the most general solution. In some cases, it is possible to use three-way or

four-way valves in order to reduce the number of components.

3.2 Parallel Connection Technology

The idea of using several hydraulic valves in parallel is probably as old as the use of hydraulic valves [8]. An early reference is Rickenbergs patent in 1930 [22] consisting of three solenoid valves each having different flow capacity. General four-way digital valve system of fig. 3.3 has been presented in the patent of Murphy and Weil in 1962 [23]. However, a few research publications can be found before 2000.

Figure 3.1(a) shows the parallel connected implementation of the two-way valve and the simplified drawing symbol is shown in fig. 3.1(b). The nickname DFCU (Digital Flow Control Unit) [8] is used for this kind of valve assembly.

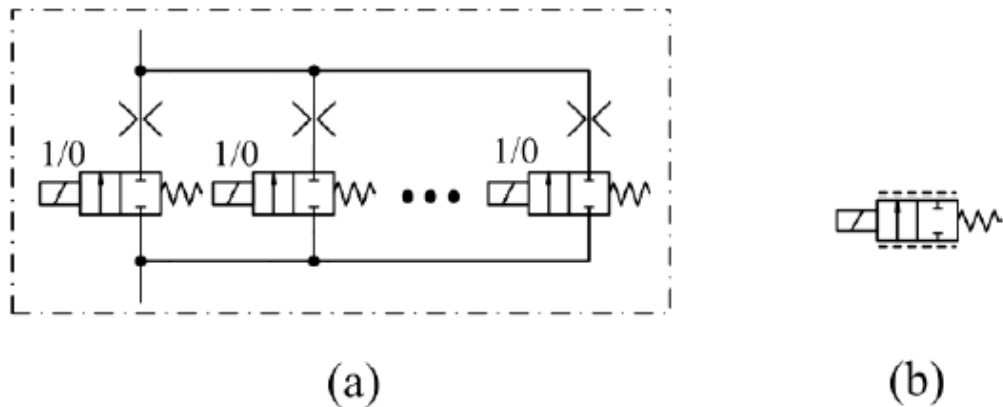


Figure 3.1: Parallel connected system (a), the simplified drawing symbol of the parallel connected system (b) [8]

Each N component of the DFCU has two distinct positions providing 2^N overall combinations which are called *states* of DFCU. Each of the *states* may give different output (e.g. flow rate) and thus the number of output values may be different from the number of the state combinations. The actual number of output values depends on the coding method, or the relative size of components. On the one hand, the smallest number of output values is achieved by using components with the same size, and the number of output values is $N+1$ (Pulse Number Modulation, PNM coding). On the other hand, the extreme is binary coding in which each *states* gives singular output values [8].

An important feature of the parallel connected systems is that no switching is needed in order to maintain any of the discrete output values. Once the state combination is selected and the control valves have achieved their positions, the output remains constant without any further actions. Some valve switchings are needed only when the state combination changes.

Figure 3.2 shows the relative output of the DFCU for different number of valves and for binary and PNM coding. The resolution improves when binary coding is used, manifesting a very accurate control with relatively few valves. The PNM has poor resolution but efficacy compensation of the faults in valve.

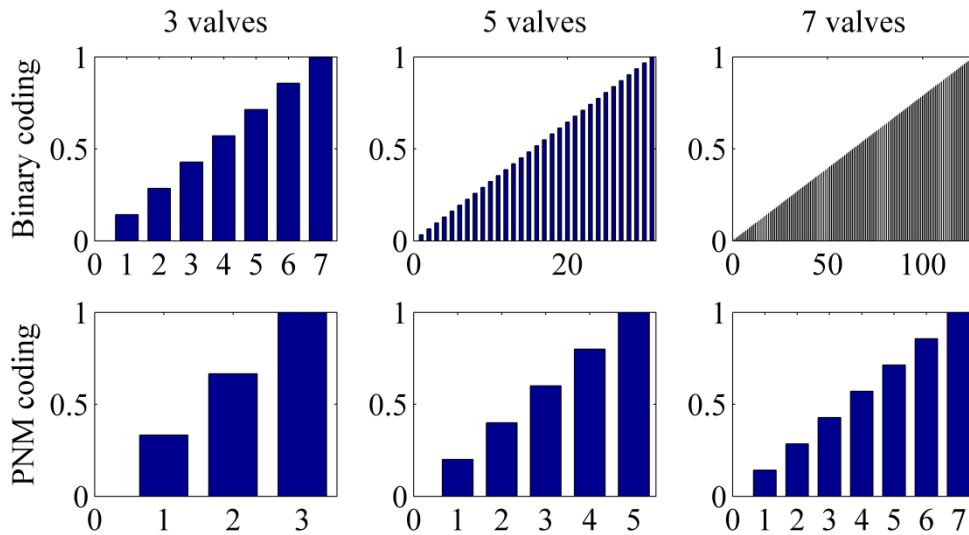


Figure 3.2: Relative DFCU output for 3, 5 and 7 valves with binary and PNM coding [8]

The implementation of a good four-way valve functionality requires 4x5 valves when binary coding is used and about 4x30 valves when PNM coding is used [8] (see figure 3.3). The larger number of components, when compared to traditional systems, seems to bring disadvantages, but it is important to consider the whole system. A mobile proportional valve consists of pressure compensator, main spool, two pilot valves, pilot pressure circuitry, and a number of springs and damping orifices. It also requires counterbalance valve in order to work properly with overrunning loads. The digital solution has 20-120 identical zero-leak valves with simple control electronics and the control code implements all the functionality. This means large number of similar components and mass production can be applied, which reduces

the price per valve [8].

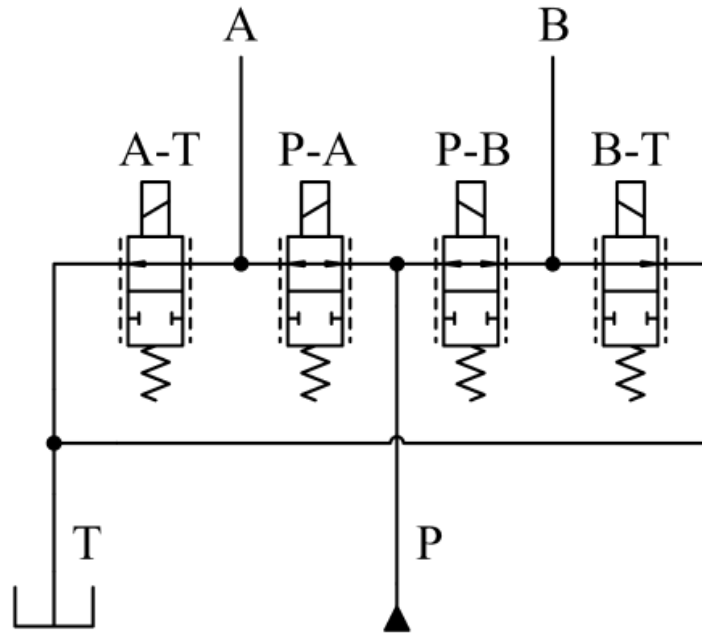


Figure 3.3: the implementation of distributed four-way valve by DFCU [8]

3.3 Switching Systems

Figure 3.4 presents the implementation of switching controlled two-way valve. It controls the average flow area by the high frequency modulation and the pulse-width modulation (PWM) is the most common approach.

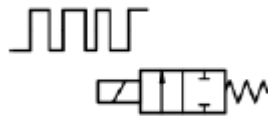


Figure 3.4: Switching controlled valve by PWM [8]

In theory, the average flow area can have any value, but finite valve dynamics limits the smallest and biggest possible duty ratio [8].

The fundamental characteristic of switching systems is that only few output values are available and the mean output is adjusted by continuous switching. Continuous switching causes noise, which can be reduced by the careful design and/or damping devices.

Historically, the most widely used and also one of the first applications of the switching valve control are the ABS brakes of cars [24]. Despite that, in the traditional hydraulics, the applications of switching control have been rare. Nonetheless, in the last decade, the subject has been aim of research again as an alternative for increasing energy efficiency, as can be seen below where one of the major applications is described.

3.3.1 The switched inertance system

A switched inertance hydraulic system (SIHS), is one possible approach to rise efficiency [25]. It was introduced in the 1980s by F.Brown as an energy conservative control and improved in the last years by researchers as Manhartsgruber et al. [26], Kogler and Scheidl [27], Hettrich et al. [28], Johnston [25] and De Negri et al. [29].

The principles of such a system are based on the cyclical acceleration and deceleration of fluid using pulse-width modulation. As discussed by Brown [30], even though the SIHS was developed independently of electrical switched power converters, the concepts are the same and analogies exist between them. The technique takes advantage of the inherent reactive behaviour of hydraulic components. A fluid volume may represent a capacity, whilst the inductance effect is reproduced by a small diameter line [25].

Next different configurations of SIHSs are introduced.

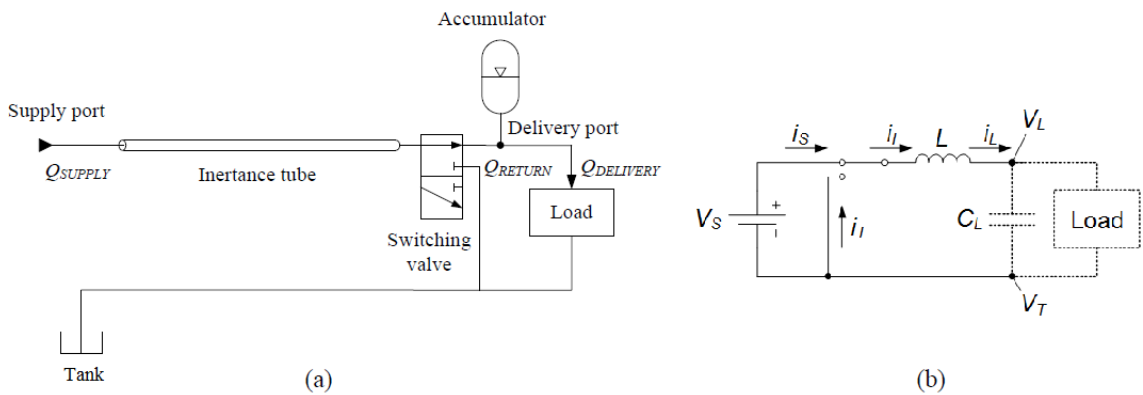


Figure 3.5: Pressure Booster: a) Hydraulic circuit; b) Electrical circuit

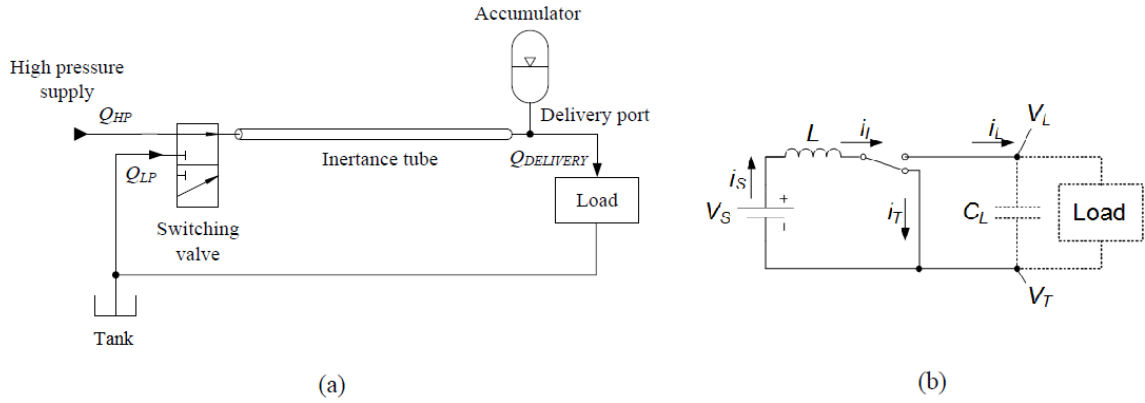


Figure 3.6: Flow Booster: a) Hydraulic circuit; b) Electrical circuit

On the one hand the electrical circuit shown in figure 3.5(b) presents the output voltage higher than the input voltage. As a result, in accordance with the electric-hydraulic analogy, the corresponding hydraulic system presented in figure 3.5(a) acts as a pressure control valve (Pressure Booster).

On the other hand, in the electrical analogy proposed in figure 3.6(b) the output current is proportional to the input voltage, and vice-versa. Therefore, the hydraulic system presented in figure 3.6(a) operates as a flow control valve (Flow Booster).

In both systems, the switching valve is driven by a pulse-width modulated (PWM) signal such that it switches cyclically and rapidly, modulating the time in which each flow path remains active.

In the Pressure Booster, when the supply is connected to the tank the internal pressure decreases and the fluid is accelerated through the tube. By the time the valve switches to the other position, the fluid momentum in the tube causes the internal pressure to increase and, consequently, the load pressure increases as well. Next, the valve switches again blocking the load port while the fluid is accelerated. That process is endlessly repeated several times per second, thus theoretically the load pressure can be modulated from the supply pressure value to infinity achieving twice the supply pressure for a duty (λ) of 50% [29].

The Flow Booster has the tube installed between the valve and the external load port. When the supply is connected to the load, the internal pressure tends to increase and, consequently, the fluid accelerates through the tube. By the time the valve switches, even though the load is linked to the tank the fluid momentum causes the fluid to continue to move through the tube, drawing the fluid from the

tank despite the adverse (low to high) pressure gradient.

The intention for switching control is to avoid the intrinsic high energy losses which occur when conventional valve-controlled systems are used. Theoretically the SIHS is lossless, but in practice losses due to friction and leakage may be significant [25]. Still, the higher efficiency and wider bandwidth than the conventional valve controlled system are the main benefits of switching control.

The design and performance of the high-speed switching valve is very important for the performance of the SIHS. The valve ideally should have low resistance and low leakage and be able to operate with a very high switching frequency [25].

The other major element is the inertance tube, which has ideally only inductance effect (L), but hydraulic resistance (R) and capacitance (C) are also included in practical systems, as represented in figure 3.7.

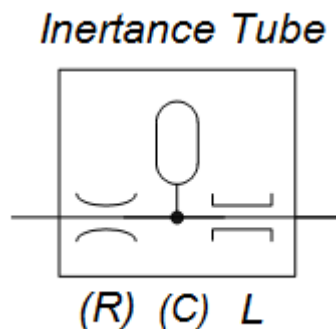


Figure 3.7: Real inertance tube

3.4 A comparison between digital fluid power and traditional systems

The research has demonstrated that digital fluid power has some advantages when compared to traditional systems. The benefits are here reported:

- robust and simple components
- faster valves which confers better performances
- control units regulate the characteristic instead of features, for example the valve spool

- entirely new configurations are possible

the digital fluid power not only brings profits, but also some challenges which are listed below:

- noise and pressure pulsation
- durability and life time with the switching technology
- physical size and price with the parallel connections
- complicated and non-conventional control

In order to apply the advantages of digital fluid power to a specific system, a technique has to be chosen. As introduced in section 3.2, the parallel connection technology exploits a large number of valve for granting a considerable range of possible flow rate values. On the other hand, the switching technology needs only single valve and the “digital effect” depends on the control unit.

For these reasons, in order to design a digital system for pitch control the parallel technique has been left aside and the efforts have concentrated on the switching technology which has theoretical advantages in term of space occupied.

3.5 The digital hydraulic system for pitch control

The developed system is presented in figure 3.8.

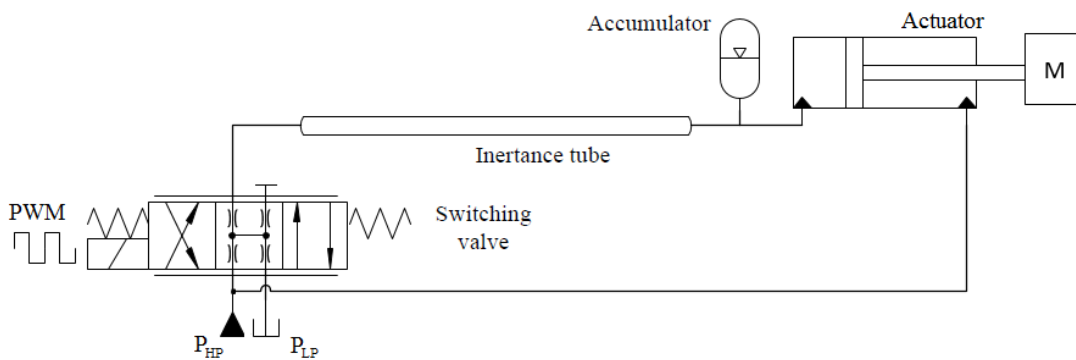


Figure 3.8: Hydraulic circuit diagram

It consists of a linear actuator, an accumulator, an inertance tube and a switching valve. Moreover, its configuration and functioning are analogue to the flow booster system described in section 3.3.

At the Laboratory of Hydraulic and Pneumatic Systems of the Federal University of Santa Catarina in Florianopolis (LASHIP), where this project has been carried out, is present a workbench for testing the hydraulic system applied on HAWTs for the blade pitch control. That test bench utilizes cylinders Bosch Rexroth CDT3MT4 series which require high pressure and flow rate for their motion. Those are conditions which limit the application of the circuit.

Although plenty of research groups, Prof. Sheidl's group among the others [31], have developed several different fast switching valve prototypes, the current 2-positions fast valves are not able to satisfy the flow rate and pressure demanded by the application.

It has been introduced the biggest obstacle to the application of digital hydraulics: the lack of the necessary valves. Thus, there is an urgent demand for good and fast switching valves, valve packages and control electronics.

These factors motivate the use of the proportional directional valve series *DFplus* D1FP from Parker Hannifin as switching valve. That valve is the best comprise present in commerce between high nominal flow rate, which is required by the actuator, and short time response, necessary for switching rapidly the valve.

As it can be seen in figure 3.8, the valve is commanded via electric signal. For commanding the valve via a pulse-width modulation and take advantage of the switching technology, it is necessary to introduce a specific control unit.

The next chapter describes in details each component of the system introduced in this section, including the control unit. Moreover, it presents the analytical models along with the modelling in the software *Simulink*

4

Modelling of the hydraulic system

The next sections illustrate the non-linear behaviour of the hydraulic system presented in section 3.5. For better comprehension, the components are here separately presented. Each section describes the performances of the element and introduces its mathematical model, which consists of a set of equations governing its dynamic behaviour according to the physical characteristics of the component.

4.1 Hydraulic Cylinder

In order to describe the performances of the hydraulic cylinder, two equations need to be introduced: the equation of motion (Newton's second law) and the continuity equation which is consequence of the mass conservation law (see [10]).

4.1.1 Equation of motion

In accordance with figure 4.1, the main forces acting on the actuator are the inertial force, which considers the accelerated mass of the system, the forces generated from the pressure acting on the piston surfaces, the external force of the load, friction forces and the spring force. The equation which regulates the motion of the cylinder is reported next:

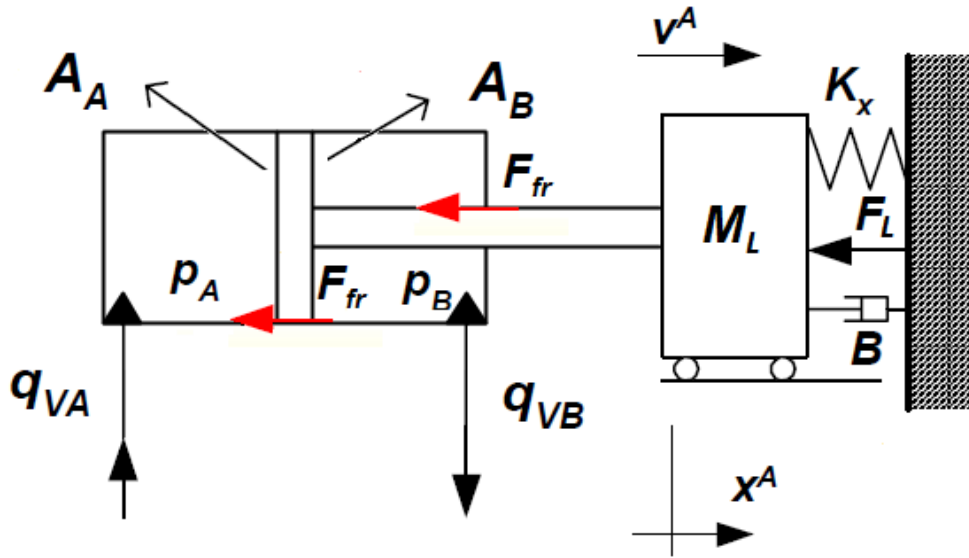


Figure 4.1: Forces acting on the cylinder

$$(A_A \cdot p_A) - (A_B \cdot p_B) = M_t \cdot \frac{d^2x}{dt^2} + B \cdot \frac{dx}{dt} + K_x \cdot x + F_{fr} + F_L \quad (4.1)$$

where

$(A_A \cdot p_A)$ is the force applied on the area A_A caused by the pressure p_A present in the chamber A;

$(A_B \cdot p_B)$ is the force applied on the area A_B caused by the pressure p_B present in the chamber B;

F_{fr} is the friction force acting on the cylinder as a combination of the static and Coulomb friction

F_L is the force applied as load

M_t is the total mass of the system.

It is composed by the external mass of the load (M_L), the mass of the cylinder (piston and rod, M_{cyl}) and fluid M_f ; thus:

$$M_t = M_L + M_{cyl} + M_f$$

B is the damping coefficient

K_x is the spring constant

The implementation in the software *Simulink* of the above equation is here reported:

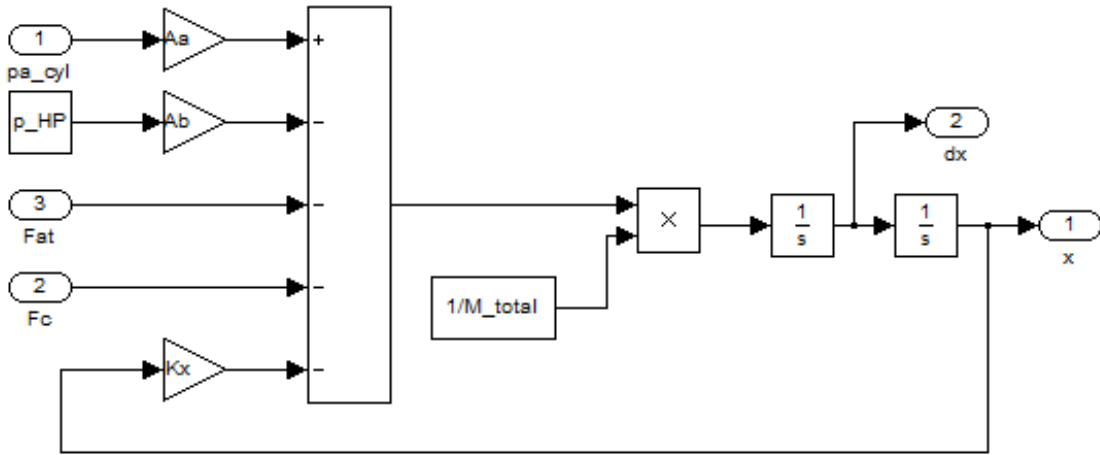


Figure 4.2: Simulink diagram of the equation of motion

4.1.2 Friction Force

The cylinder is affected by a friction force which obstacles the movement. The characteristic of this force has been widely matter of study in the literature and several models exist for describing its behaviour. In particular for this case of study, the model proposed by Gomes has been used [32]. This model, as displayed in figure 4.3, defines three regions: the curve C-D, which identify the *stick* region where the applied force has a smaller absolute value than the friction static force F_{sp} , the region *slip* (curve B) where the applied force has a greater value than F_{sp} and the curve A where the velocity is greater than the limit value (\dot{x}_{lim}). The velocity (\dot{x}_{lim}) is defined as the lower limit value at which the cylinder velocity is constant. Below the (\dot{x}_{lim}) the cylinder has an intermittent motion stops and slips (*stick-slip*)

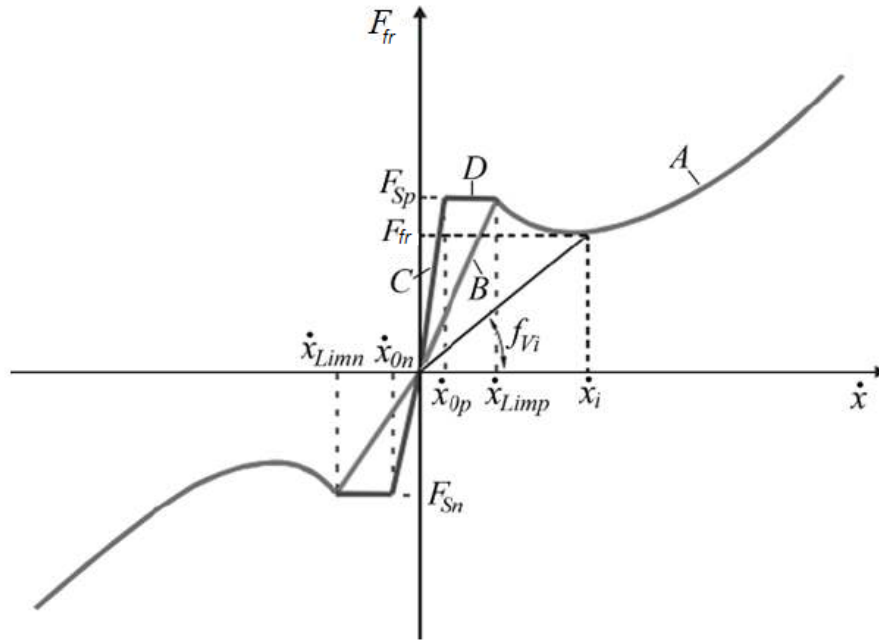


Figure 4.3: Diagram of the Gomes friction model [9]

The characteristic of the curves of the cylinder used for this study had been evaluated by experimental assessments [14].

4.1.3 Continuity Equation

It is a stronger and local form of the conservation of mass law. For incompressible flows and a *control volume* (V), which is an imaginary surface enclosing a volume of interest, the equation can be written as: [33]

$$Q_1 - Q_2 = \frac{dV}{dt} + \frac{V}{\beta_e} \cdot \frac{dp}{dt} \quad (4.2)$$

where

Q_1 is the flow in the control volume [m^3/s]

Q_2 is the flow out the control volume [m^3/s]

$\frac{dV}{dt}$ is the rate of change of the volume V [m^3/s]

β_e is the effective bulk modulus [Pa]

$\frac{dp}{dt}$ is the rate of pressure change occurred within the volume V [Pa/s]

In practice the latter term, considers the eventual compression or expansion of the fluid into the control volume.

Considering now the control volume V as the internal volume V_A of the cylinder, as shown in figure 4.4, the continuity equation can be expressed as: [10]

$$q_{VA} = -q_{vin} + \frac{dV_A}{dt} + \frac{V_A}{\beta_e} \cdot \frac{dp_A}{dt} \quad (4.3)$$

where

q_{VA} is the flow in the chamber A of the cylinder [m^3/s]

q_{vin} is the internal leakage between the chambers A and B of the cylinder [m^3/s]

V_A is the internal volume of chamber A [m^3]

p_A is the internal pressure in chamber A [Pa]

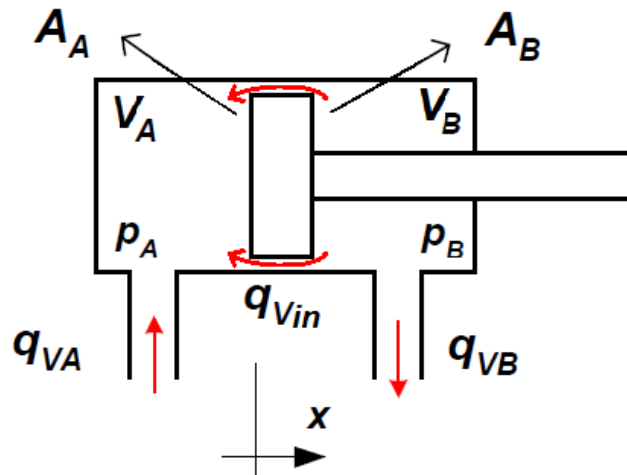


Figure 4.4: Continuity equation for the double-acting hydraulic cylinder

The internal leakage q_{vin} is a parameter that contributes in increasing the damping (ξ) of the system. The leak is expressed as a linear function that varies in proportion to the difference pressure between the cylinder chambers [34]:

$$q_{vin} = C_{in} \cdot (p_B - p_A) \quad (4.4)$$

where

C_{in} is the internal leakage constant [$\frac{m^3}{s \cdot Pa}$]
 p_B is the internal pressure of chamber B [Pa]

The equation 4.3 can be written analogously for the chamber B:

$$q_{VB} = -q_{Vin} + \frac{dV_B}{dt} + \frac{V_B}{\beta_e} \cdot \frac{dp_B}{dt} \quad (4.5)$$

where

q_{VB} is the flow rate coming out from the chamber B of the cylinder [m^3/s]
 V_B is the internal volume of chamber B [m^3]
 p_B is the internal pressure in chamber B [Pa]

Figure 4.4 points out that the volumes V_A and V_B depend on the displacement (x) of the piston. As a result, the following relationships can be defined:

$$\begin{aligned} V_A &= V_{A0} + A_A \cdot x & V_B &= V_{B0} - A_B \cdot x \\ \frac{dV_A}{dt} &= A_A \cdot v = A_A \cdot \frac{dx}{dt} & \frac{dV_B}{dt} &= -A_B \cdot v = -A_B \cdot \frac{dx}{dt} \end{aligned} \quad (4.6)$$

where

V_{A0} is the internal volume of chamber A by the time $x = 0$ [m^3]
 V_{B0} is the internal volume of chamber B by the time $x = 0$ [m^3]
 A_A is the area of the piston at the chamber A side [m^2]
 A_B is the area of the piston at the chamber B side [m^2]

Moreover, the chamber B of the cylinder is directly connected to the high pressure port of the power unit thus the rate of change of the pressure p_B is equal to 0 and $p_B = p_{HP}$. Therefore the equations 4.5 and 4.4 can be modified as:

$$q_{VB} = -q_{Vin} - A_B \cdot \frac{dx}{dt} \quad (4.7)$$

$$q_{Vin} = C_{in} \cdot (p_{HP} - p_A) \quad (4.8)$$

Using the equations 4.6 it is also possible to re-write the equation 4.3 in a form able to establish the rate of change over time of the internal pressure p_A :

$$\frac{dp_A}{dt} = \frac{\beta_e}{V_{A0} + A_A \cdot x} \cdot [q_{VA} + C_{in} \cdot (p_{HP} - p_A) - A_A \cdot \frac{dx}{dt}] \quad (4.9)$$

The implementation in the software *Simulink* of the above equation is here reported:

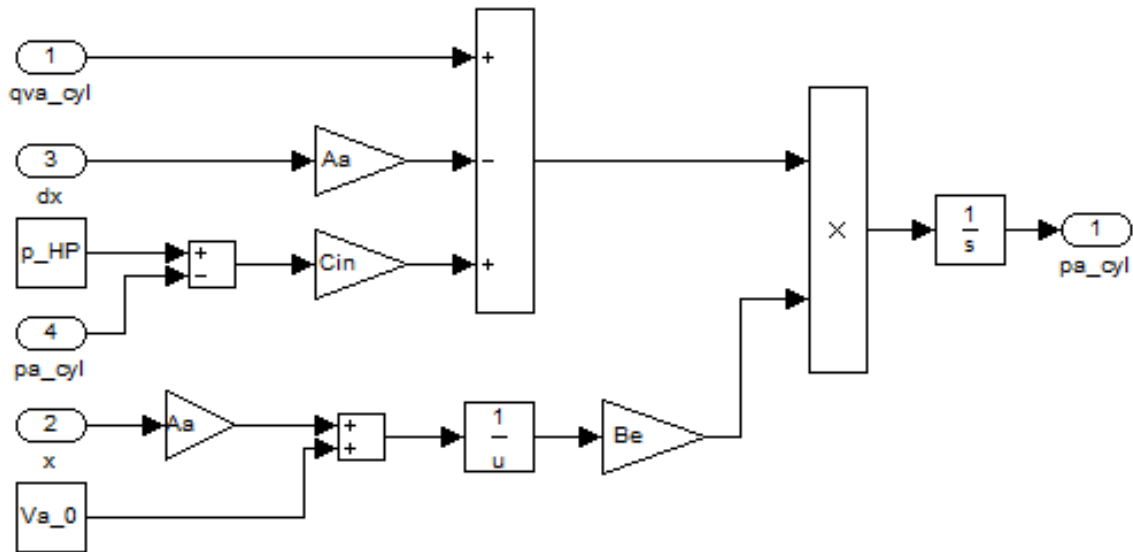


Figure 4.5: Simulink diagram of the continuity equation for the cylinder

4.2 Proportional Directional Valve

The valve D1FP from Parker Hannifin is hereafter described.

First, the performances of the valve as a proportional device are introduced. Second, the component acting as a switching valve is taking in consideration.

4.2.1 Proportional Valve

The term “proportional valve” defines a valve able to shift its spool with continuity in a number of infinitive positions generating a variable output (i.e. flow rate) which has the value proportional to the spool displacement.

As can be seen in the diagram 3.8, the valve is commanded electrically by exciting the solenoid coil. It exists therefore, an electrical signal acting on the solenoid which regulates the spool displacement, and consequently, the flow rate of the valve. The entity of the flow rate depends on the intensity of the current transmitted to the solenoid by a control signal U_c expressed in voltage.

In our case the D1FP valve is commanded by a signal control $-10 \leq U_c \leq +10$; where $U_c = +10$ corresponds to the complete opening and closing of the orifices 3 and 4 respectively, as a result of emitting the maximum flow ($P_{HP} > P_A$); and $U_c = -10$ matches the opposite situation, as can be seen in fig. 4.6.

The D1FPseries contains four-way valves, but according to the figure 3.8 the case of this study uses the device with one of its port blocked, thus the component can be considered as a three-way valve. For this reason, henceforth the analysis and discussions are only about a three-way valve in order to reduce the complexity of the study.

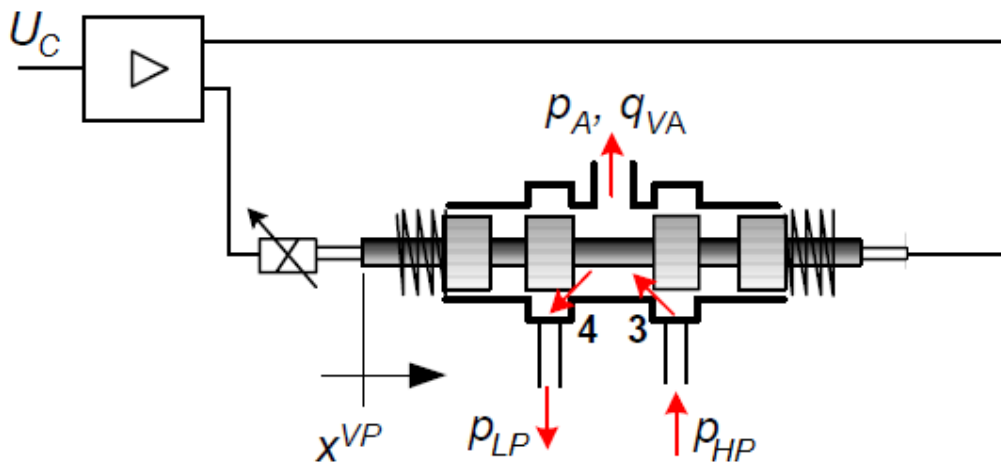


Figure 4.6: Intern of a three-way valve, [10]

When $x^{VP} = 0$ the orifices 3 and 4 are closed by the spool which blocks the emission of fluid; as the displacement x^{VP} assumes positive values, the spool moves

forward freeing the orifice 3 to an extent proportional to the signal control. Analogue but opposite mechanism happens when x^{VP} assumes negative values. Using the modified Bernoulli's equation valid for orifices and steady state conditions

$$q_V = cd \cdot A_0 \cdot \sqrt{\frac{2\Delta p}{\rho}} \quad (4.10)$$

the mathematical description of the phenomena is illustrate as followed:

$$q_{VA} = cd \cdot A_3 \cdot \sqrt{\frac{2}{\rho}(p_{HP} - p_A)} - cd \cdot A_4 \cdot \sqrt{\frac{2}{\rho}(p_A - p_{LP})} \quad (4.11)$$

where

- cd is the coefficient of the orifices
- $A_{3,4}$ is the area of the orifices [mm^2]
- p_{HP} is the high pressure [Pa]
- p_{LP} is the low pressure [Pa]

Notice that the notation convection considers positive the flow rate running out from the valve towards the actuator.

The flow coefficient

The coefficient cd and areas $A_{3,4}$ vary as a function of the spool displacement x^{VP} ; it occurs then problems related to their determination. For this reason, another parameter is introduced [10]:

$$K_v = \frac{q_{Vn}}{\sqrt{\Delta p_n}} \quad (4.12)$$

where

K_v is the flow coefficient $[(m^3/s)/(Pa)^{1/2}]$

q_{Vn} is the nominal flow rate of the valve $[m^3/s]$

Δp_n is the nominal pressure difference, at which q_{Vn} is determined [Pa]

The new parameter is easier to determinate from the data sheet of the component than the ones before. Now, considering the coefficient cd and the areas $A_{3,4}$ equals for both the orifices, the K_v can be considered as unique and equation 4.11 re-defined as followed:

For $x^{VP} \geq 0$:

$$q_{VA} = K_v \cdot \frac{U_c}{U_n} \cdot \sqrt{p_{HP} - p_A} \quad (4.13)$$

For $x^{VP} < 0$:

$$q_{VA} = -K_v \cdot \frac{|U_c|}{U_n} \cdot \sqrt{p_A - p_{LP}} \quad (4.14)$$

where

U_c is the control signal [V]

U_n is the nominal control signal [V]

The D1FP valve chosen for the application has a zerolap spool type, as shown in figure 3.8, thus the leakage of the valve assumes high relevance in order to determinate the valve dynamics and desired flow rate. For this reason, the parameter K_{vin} , which considers the leakage of the valve, is introduced in eq. 4.13 and eq. 4.14:

For $x^{VP} \geq 0$:

$$q_{VA} = (K_v \cdot \frac{U_c}{U_n} + K_{vin}) \cdot \sqrt{p_{HP} - p_A} - K_{vin} \cdot \sqrt{p_A - p_{LP}} \quad (4.15)$$

For $x^{VP} < 0$:

$$q_{VA} = -\left(K_v \cdot \frac{|U_c|}{U_n} + K_{vin}\right) \cdot \sqrt{p_A - p_{LP}} + K_{vin} \cdot \sqrt{p_{HP} - p_A} \quad (4.16)$$

where

K_{vin} is leakage flow coefficient $[(m^3/s)/(Pa)^{1/2}]$

Notice that based on the observation of equals orifices and coefficient cd , the parameter K_{vin} is unique as K_v is. The leakage flow coefficient K_{vin} can be determined as followed:

$$K_{vin} = \frac{qv_p}{\sqrt{2} \cdot p_s} \quad (4.17)$$

where

qv_p is the leakage flow rate present in the catalogue [ml/min]

p_s is pressure at which qv_p is obtained [Pa]

The implementation of the model expressed by the equations 4.15 and 4.16, is illustrated in the figure below:

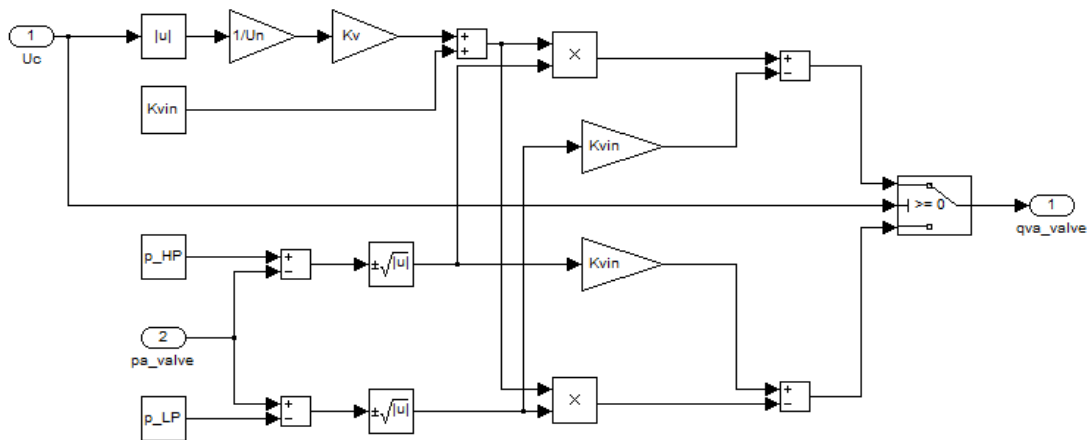


Figure 4.7: Simulink diagram of the proportional valve

4.2.2 Switching Valve

In order to command the valve as a switching device, a pulse generator needs to be applied. As illustrated in the previous section, the valve package accepts an electrical signal which ranges from -10 to +10 V. Then these two limits are the outputs of the pulse wave. The pulse wave is a kind of non-sinusoidal waveform that is similar to a square wave, but does not have the symmetrical shape associated with a perfect square wave. The parameters which define a pulse wave are the frequency (f) which is the inverse of the period (T), and the duty cycle (λ), which represents the pulse duration during T . In addition, the duty cycle can be modulated for a more dynamic response; that is the case of this study and it is called pulse-width modulation (PWM).

Switching the valve at high-frequency using the PWM, installs in the system phenomena characterized by the inertia of the fluid as described in section 3.3. When the valve communicates with the high pressure the pressure p_A tends to increase and the fluid accelerates through the tube; when the switching occurs the port A is connected to the lower pressure port but the fluid momentum causes the fluid to continue to move through the tube, drawing the fluid from the tank port despite the adverse (low to high) pressure gradient. Thus, the equations 4.15 and 4.16 can be modified as followed:

For $x^{VP} \geq 0$:

$$q_{VA} = (K_v + K_{vin}) \cdot \sqrt{p_{HP} - p_A} + K_{vin} \cdot \sqrt{p_{LP} - p_A} \quad (4.18)$$

For $x^{VP} < 0$:

$$q_{VA} = (K_v + K_{vin}) \cdot \sqrt{p_{LP} + p_A} - K_{vin} \cdot \sqrt{p_{HP} - p_A} \quad (4.19)$$

As can be seen in the above equations, the term $\frac{U_c}{U_n}$, which represents to what extent the spool opens the orifices, has been removed coherently with the PWM control. However, in practice the valve is affected by some dynamical effects which impede

the valve to switch instantly from one extreme position to the opposite one; therefore the signal control U_c varies rapidly from -10V to +10V and vice-versa, but it is not able to assume only those values at every instants. For this reason, the equations 4.18 and 4.19 have to be re-written as:

For $x^{VP} > 0$:

$$q_{VA} = (K_v \cdot \frac{U_c}{U_n} + K_{vin}) \cdot \sqrt{p_{HP} - p_A} + K_{vin} \cdot \sqrt{|p_{LP} - p_A|} \quad (4.20)$$

For $x^{VP} < 0$:

$$q_{VA} = (K_v \cdot \frac{|U_c|}{U_n} + K_{vin}) \cdot \sqrt{p_{LP} - p_A} + K_{vin} \cdot \sqrt{p_{HP} - p_A} \quad (4.21)$$

The described dynamical effects can be taken into account introducing a relation which expresses the dynamic response of the valve characterized by second order behaviour, then:

$$U_c = \frac{1}{\omega_n^2} \cdot \frac{d^2 x^{VP}}{dt^2} + \frac{2\xi}{\omega_n} \cdot \frac{dx^{VP}}{dt} + x^{VP} \quad (4.22)$$

and using the Laplace transform, the transfer function results:

$$\frac{X^{VP}(s)}{U_c(s)} = \frac{\omega_n^2}{s^2 + 2\xi\omega_n s + \omega_n^2} \quad (4.23)$$

where

ω_n is the natural frequency of the valve

ξ is the damping ratio

For the simulations a damping ratio equal to 0.9 has been used. Moreover, the catalogue Parker Hanninfin of the valve D1FP indicates a time response <3.5 ms that becomes 7 ms considering the switching from one position to the opposite one,

thus the natural frequency of the valve is equal to

$$\omega_n = 2\pi f = \frac{2\pi}{T} = \frac{2\pi}{0.007} = 897.6[\text{rad/s}] \quad (4.24)$$

The implementation of the switching valve model expressed by the two latter equations, is illustrated in the figure below:

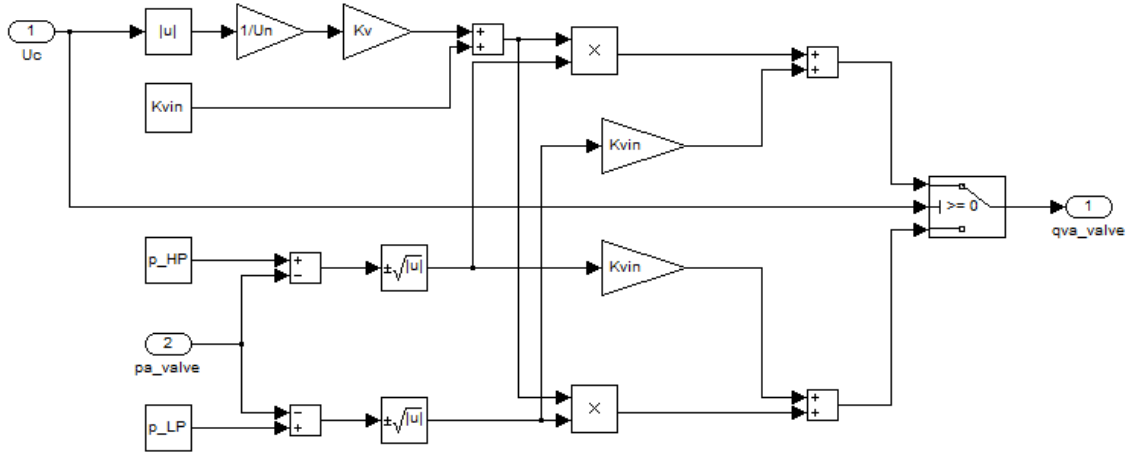


Figure 4.8: Simulink diagram of the switching valve

4.3 Inertance Tube

The flowrate $q(t)$ in the time domain at the connection between the valve and the inertance tube can be obtained by using Fourier series [11]:

$$q(t) = 2 \sum_{n=1}^{\infty} Q_n \exp \frac{jn2\pi t}{T} + q_m \quad (4.25)$$

where q_m is the mean delivery flow rate and T is the switching cycle period. An example of the predicted flow rate is shown in figure 4.9. Pulsations due to wave transmission effects can be seen clearly; the precise shape of the flow rate waveform will depend on several factors including the tube length and switching frequency.

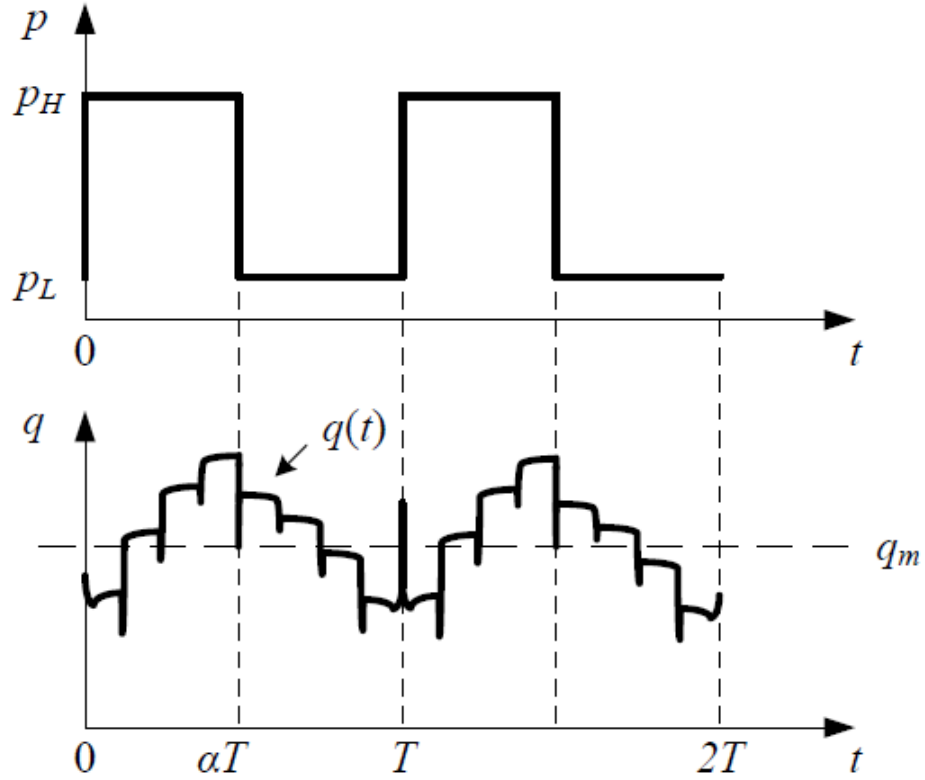


Figure 4.9: Supply pressure and example of flow rate with an ideal instantaneous switching transition [11]

The Transmission Line Method (TLM) was used to model the wave propagation in the tube. The model was developed by Krus et al [35] and modified by Johnston [15] to include unsteady or frequency-dependent friction. This model accurately and efficiently represents wave propagation and laminar friction over a very wide frequency range. However, the previous TLM models have some inherent inaccuracies [35, 15]. An improved alternative TLM model has been proposed by Johnston [36], and it was used in the following simulation work.

The efficiency of a SIHS depends on the tube diameter and length. According to the studies conducted by De Negri et al.[37] the best performances could be achieved using a tube of length 20 m, which is unfortunately unsuitable for real applications. Thus, the best practicable option resulted in a tube of length 6 m and diameter 7.1 mm, which is the tube used in the simulations and experiments.

4.4 Accumulator

Flow rate pulsation through pipelines caused by hydraulic components is one of the most common source of vibration and noise in hydraulic control systems. In order to reduce those phenomena a hydraulic damper such an accumulator needs to be applied on the circuit. Moreover, to improve the efficiency of the damping a directional component which simply drives the flow into the accumulator can be added[33]. This way the energy transmission and consequently the pulsation damping are favoured. Those advantages are shown in figure 4.10

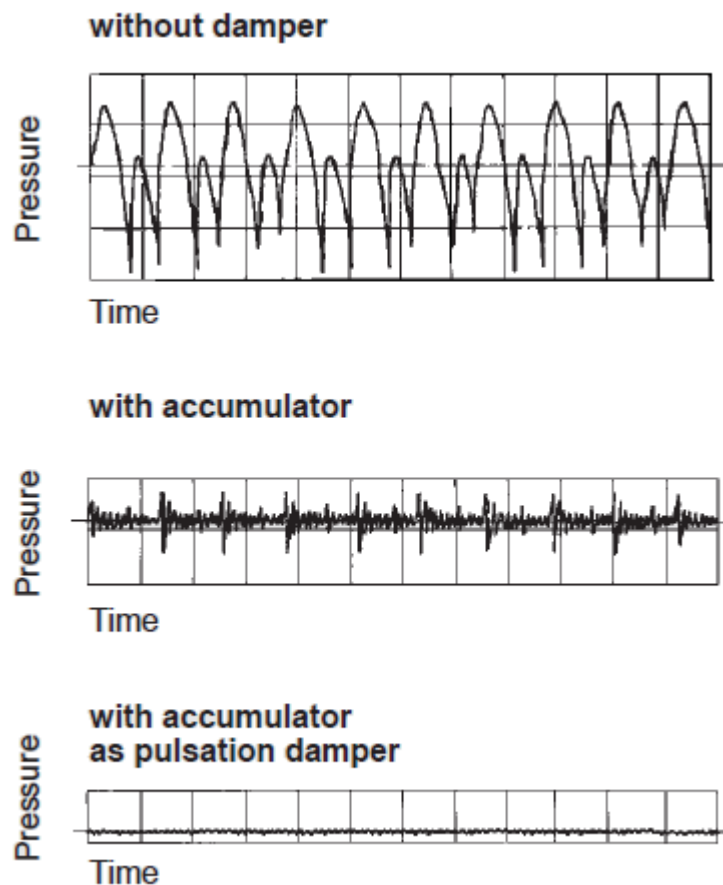


Figure 4.10: Pressure diagrams with different dampeners [12]

The three main existing types of hydraulic accumulators are weight-loaded, spring-loaded, and gas-charged (see figure 4.11). Weight-loaded and spring-type accumulators are not widely used, regardless of the simplicity of their construction and their possible fabrication using standard hydraulic cylinder barrels. This is due to their low response, large sizes, and working constraints. The most widely used

accumulators are the gas-charged types, where the oil is stored under the pressure of a gas, usually nitrogen. Gas-charged accumulators are classified into four types according to the oilgas separation: piston type, bladder type, diaphragm type, and accumulators without oilgas separation.

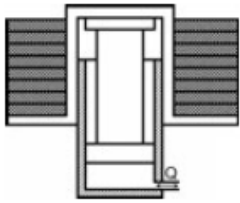
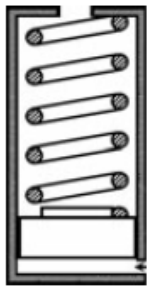

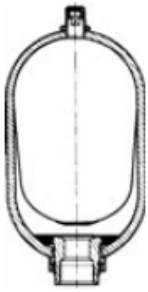

Weight-loaded	Spring-loaded	Gas-charged (with separating element)		
		Piston type	Bladder	Membrane
				

Figure 4.11: Basic types of hydraulic accumulators [13]

The accumulator used for this application is a diaphragm type, hereafter is then introduced this model and the following equations and calculations are referred to it.

Inside the accumulator a diaphragm is clamped between the walls of the pressure vessel and serves as an elastic separator between the hydraulic fluid and gas. The membrane is fixed to the pressure vessel either through welding (non replaceable), or by screwing (replaceable membrane). A shut-off button (plate) is fixed to the base of the diaphragm [13]. The processes operated by the accumulator are next schematize

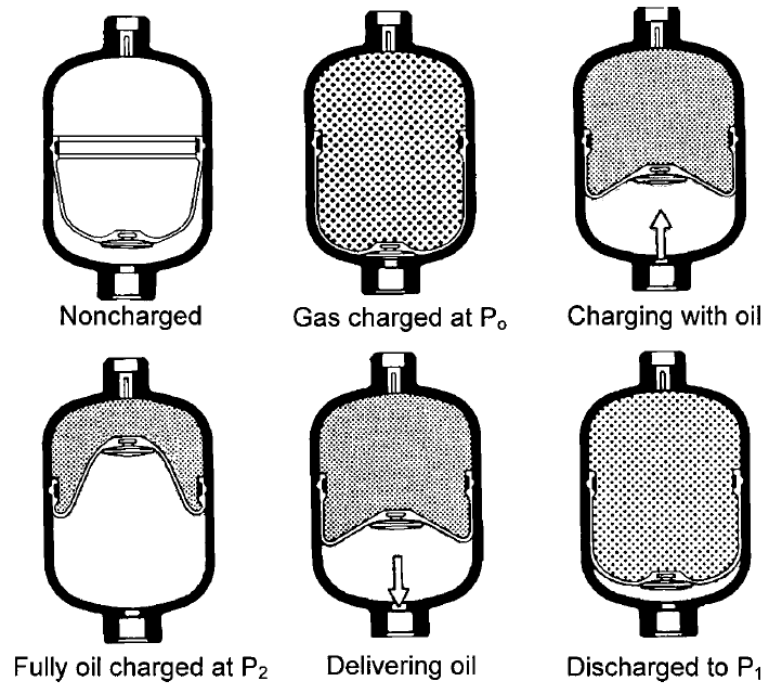


Figure 4.12: Operations of the diaphragm accumulator [13]

The following equation describes the gas compression process:

$$p_0 \cdot V_0^n = p_1 \cdot V_1^n = p_2 \cdot V_2^n = \text{const} \quad (4.26)$$

where

p_0 is accumulator charging pressure [Pa] (absolute value, abs)

p_1 is maximum system pressure [Pa] (abs)

p_2 is minimum system pressure [Pa] (abs)

V_0 is the accumulator size or capacity, volume of charging gas at pressure p_0 [m^3]

V_1 is the volume of gas at pressure p_1 [m^3]

V_2 is the volume of gas at pressure p_2 [m^3]

According to the type of compression process, the value of the exponent n varies in the range from 1 to 1.4. For an isothermal process, $n = 1$; for a polytropic process, $1 < n < 1.4$, and for an adiabatic process, $n = \gamma = 1.4$. In our case in which rapid compression or expansion occur, the heat transfer by the borders happens slow and the gas temperature varies, thus the process can be considered adiabatic.

Notice that the pressures are absolute.

Defining a variable p_g equal to the gas pressure at an instant t ; and a gas volume V_g evaluated at the same instant, the eq. 4.26 becomes:

$$p_0 \cdot V_0^\gamma = p_g \cdot V_g^\gamma = cost \quad (4.27)$$

Differentiating over time the above equation gives:

$$\frac{dV_g}{dt} = -\frac{\dot{p}_g}{\gamma \cdot p_g} \cdot V_g \quad (4.28)$$

From equation 4.27:

$$p_g = \frac{p_0 \cdot V_0^\gamma}{V_g^\gamma} \quad (4.29)$$

The variable V_g express the gas volume at an instant t , but at the same instant the volume of fluid V_f within the accumulator at the pressure p_f is:

$$V_f = V_0 - V_g \quad (4.30)$$

Considering that:

- the rate of change of the gas volume is the opposite of the rate of change of the fluid volume, $\frac{dV_g}{dt} = -\frac{dV_f}{dt}$
- the rate of change of the gas pressure is equal to the rate of change of the fluid pressure, $\dot{p}_g = \dot{p}_f$

It is possible to substitute eq. 4.29 and 4.30 into 4.28 and obtaining

$$\frac{dV_f}{dt} = \frac{(V_0 - V_f)^{\gamma+1}}{\gamma \cdot V_0^\gamma \cdot p_0} \cdot \dot{p}_f \quad (4.31)$$

Combining equation 4.30 and 4.29 the below relation is obtained:

$$V_f = \left(1 - \frac{p_0^{\frac{1}{\gamma}}}{p_f^{\frac{1}{\gamma}}}\right) \cdot V_0 \quad (4.32)$$

Considering now the fluid within the accumulator as control volume V_f , it is possible to apply the continuity equation:

$$Q_{in} - Q_{out} = \frac{dV_f}{dt} + \frac{V_f}{\beta_e} \cdot \frac{dp_f}{dt} \quad (4.33)$$

Using the equations 4.31 and 4.32 the latter relation can be modified as:

$$Q_{in} - Q_{out} = \left(\frac{1}{\gamma} \cdot \frac{(V_0 - V_f)^{\gamma+1}}{V_0^\gamma} \cdot \frac{1}{p_0} + \frac{V_f}{\beta_e}\right) \cdot \frac{dp_f}{dt} \quad (4.34)$$

where Q_{in} and Q_{out} are the flow rates coming in and out respectively from the accumulator.

At the beginning of the section has been introduced the possibility to connect at the accumulator a component able to improve the dampener efficiency, that element is here illustrated:

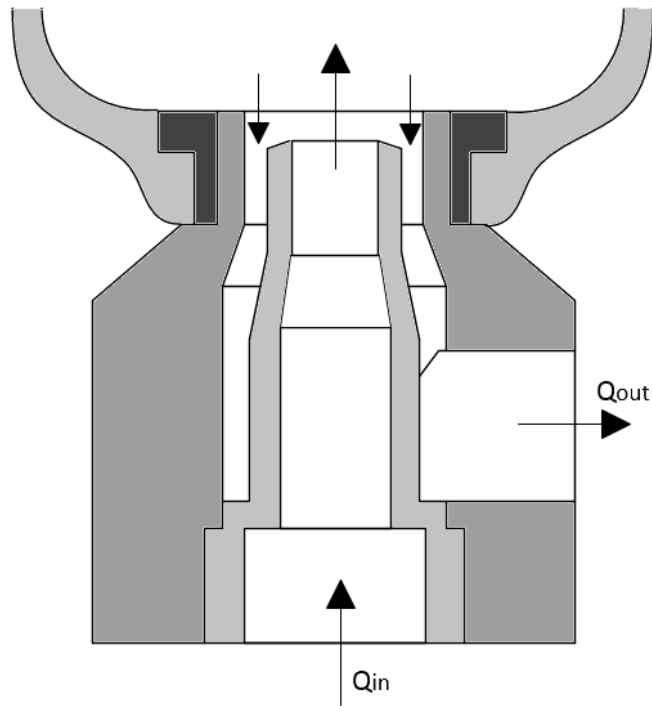


Figure 4.13: Directional component for the accumulator

Knowing the components features, in particular the areas of the orifices, makes possible determining the flow rate coming out from the accumulator using the modified Bernoulli's equation 4.10.

Exploiting the equations 4.31, 4.32 and 4.10 the analytical model of the accumulator can be implemented in the software *Simulink* as followed:

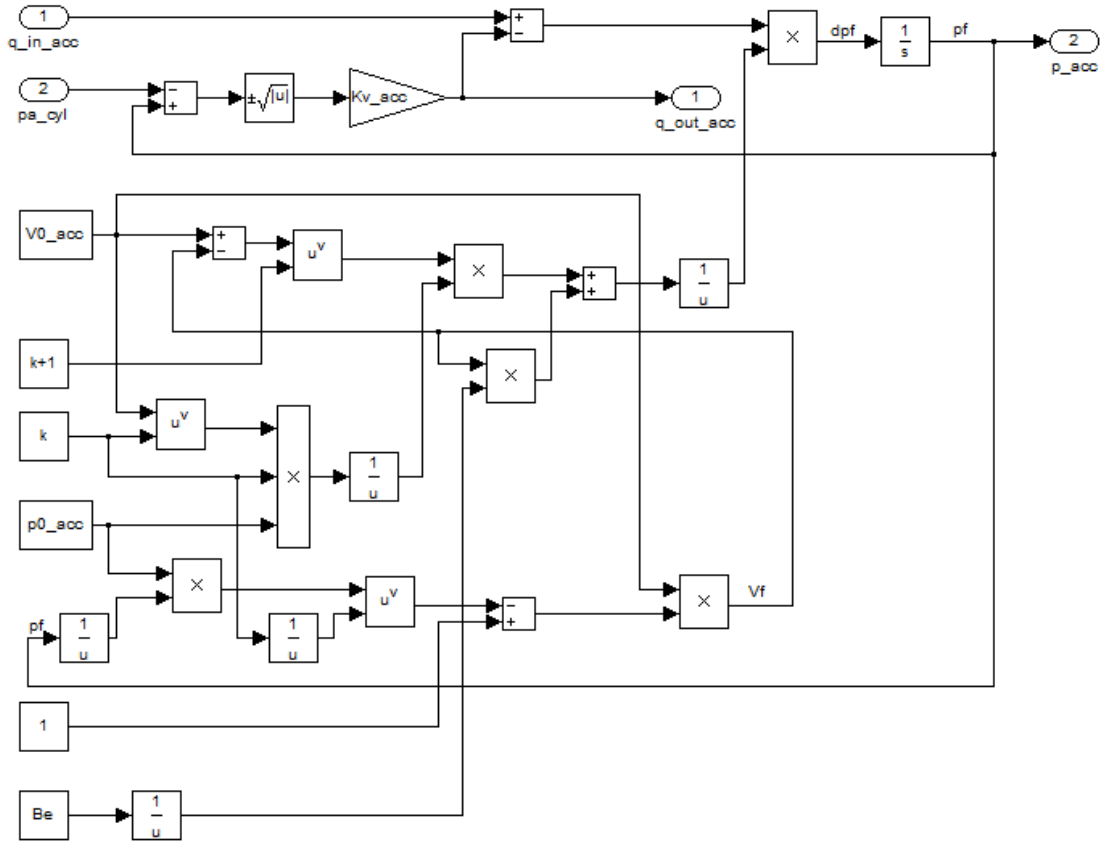


Figure 4.14: Simulink diagram of the accumulator

The accumulator has to be placed as close as possible to the source of noise. For the application regarding this study, that particular resulted in problematic related to the space occupied by the device; first for the application on the test bench and last for an eventual installation on wind turbines.

For this reason the sizing of the accumulator have been subjected to strong dimensional limitations which led to install an accumulator with the capacity of 0.32 l. The simulations guided the sizing of the accumulator, giving rapid responses of the performance variations at changing the accumulator size among the practicable capacities.

4.5 Control Unit

The applied system control is a feedback loop. it uses negative feedback which performs on the system an accurate control based on the comparison of the output with a set input. The control generates at every instant an error signal proportional to the difference among input and output which guides the latter to assume the

reference.

This technique usually pretends the presence of a PID which aids on the control of the output. It is applied after the comparison and it modifies the signal error $e(t)$ in an affine way which supports the output tracking the input. The PID algorithm involves three-term control: the proportional, the integral and the derivative with their respective constants. Tuning correctly the three parameters provide useful control action designed for specific process requirements. However, the PID does not guarantee optimal control of the system or system stability. Using the Laplace transform the PID can be represented as follows

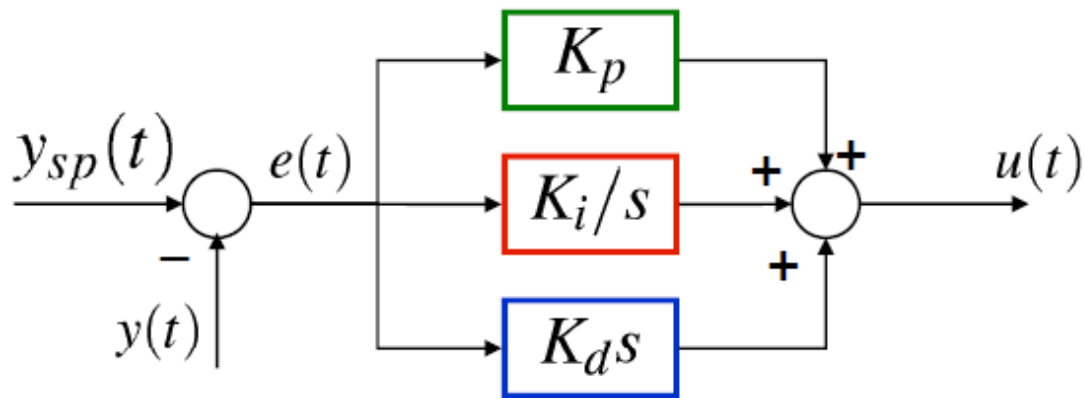


Figure 4.15: Diagram of a PID controller

$$u(t) = K_p e(t) + K_i \int e(t) dt + K_d \frac{de(t)}{dt} \quad (4.35)$$

where

K_p is the proportional constant

K_i is the integral constant

K_d is the derivative constant

$y_{sp}(t)$ is the input set point

$y(t)$ is the output signal

$e(t)$ is the signal error

$u(t)$ is the modified error

Depending on the system only one or two actions may be required in order to

provide the appropriate system control. In hydraulics the PI controllers are the most frequently used, since derivative action is sensitive to measurement noise, whereas the absence of an integral term may prevent the system from reaching its target value.

The system control used in this project is schematized as follows

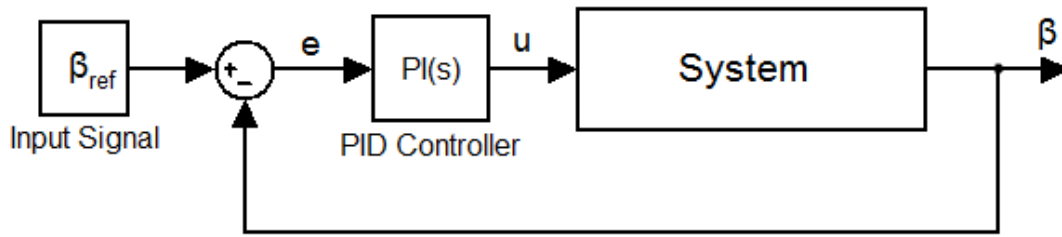


Figure 4.16: Scheme of the applied system control

To conclude, the simulink diagram of the whole SIHS is shown

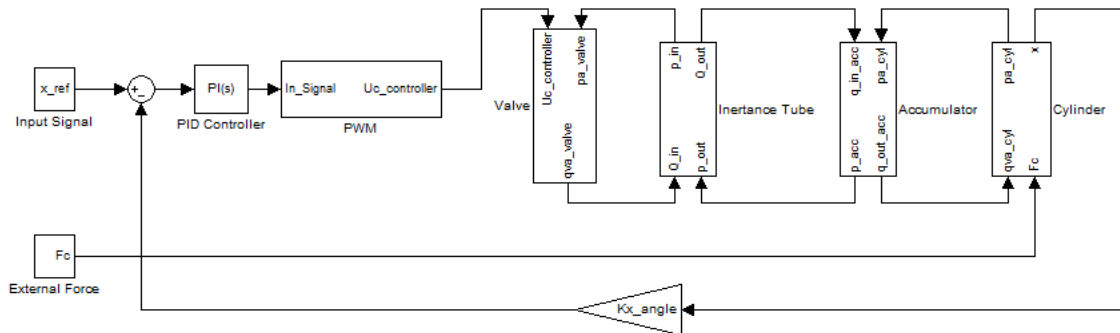


Figure 4.17: Simulink diagram of the SIHS

5

Theoretical and Experimental Results

This chapter presents the results achieved by dynamic simulations performed using the model described in the last chapter; in addition, it introduces the test bench utilized and the experimental results obtained. To conclude, an evaluation of energy savings has been proposed.

5.1 Test Bench

The workbench used for this work and located at LASHIP¹ was firstly developed in 2012 by the master's student Enrique Facundo who studied the forces submitted to pitch control systems of wind turbines [14]. Second, the master's student Marcos Nostrani modified the bench in order to study the performances of hydraulic systems for pitch control via feedback loop [38].

The author and Nostrani collaborated during the development of their works for optimizing and testing the hydraulic system proposed as object of this thesis.

In many cases, the most effective way to test a system is to connect the system to the real plant. However, in the present case the real plant imposes limitations in terms of costs and scope of the testing. For this reason the hardware-in-the-loop (HIL) simulation has been introduced by Facundo [14] for studying the pitch control system. The HIL is a technique which add the complexity of the plant under control

¹Laboratory of Hydraulic and Pneumatic Systems of the Department of Mechanical Engineering at the Federal University of Santa Catarina, Florianópolis (SC), Brazil

by adding a mathematical representation of the involved dynamic system.

HIL simulations in many cases enhances the quality of the testing since they provides the efficient control and safe environment where test engineer can focus on the functionality of the controller. In addition, they usually are more efficient than tests on real plant, in term of costs, duration, safety and practicability.

The system developed by Facundo [14] involves two hydraulic cylinders: one designed for regulating the blade pitch, whereas the other emulates the wind phenomena via HIL applying a specific force to the blade. The system is shown in figure 5.1 and 5.2.

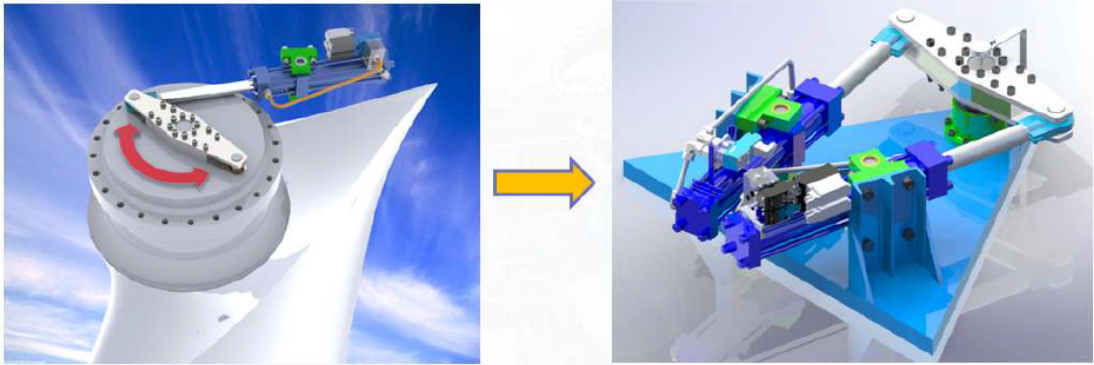


Figure 5.1: Application of the HIL [14]

The next figure shows the principal components of the test bench: the blade, the two cylinders respectively commanded by the D1FP valve and two pressure reduction valves, the inertance tube and an encoder which gives the angular position of the blade utilized as output signal of the feedback loop (see section 4.5).

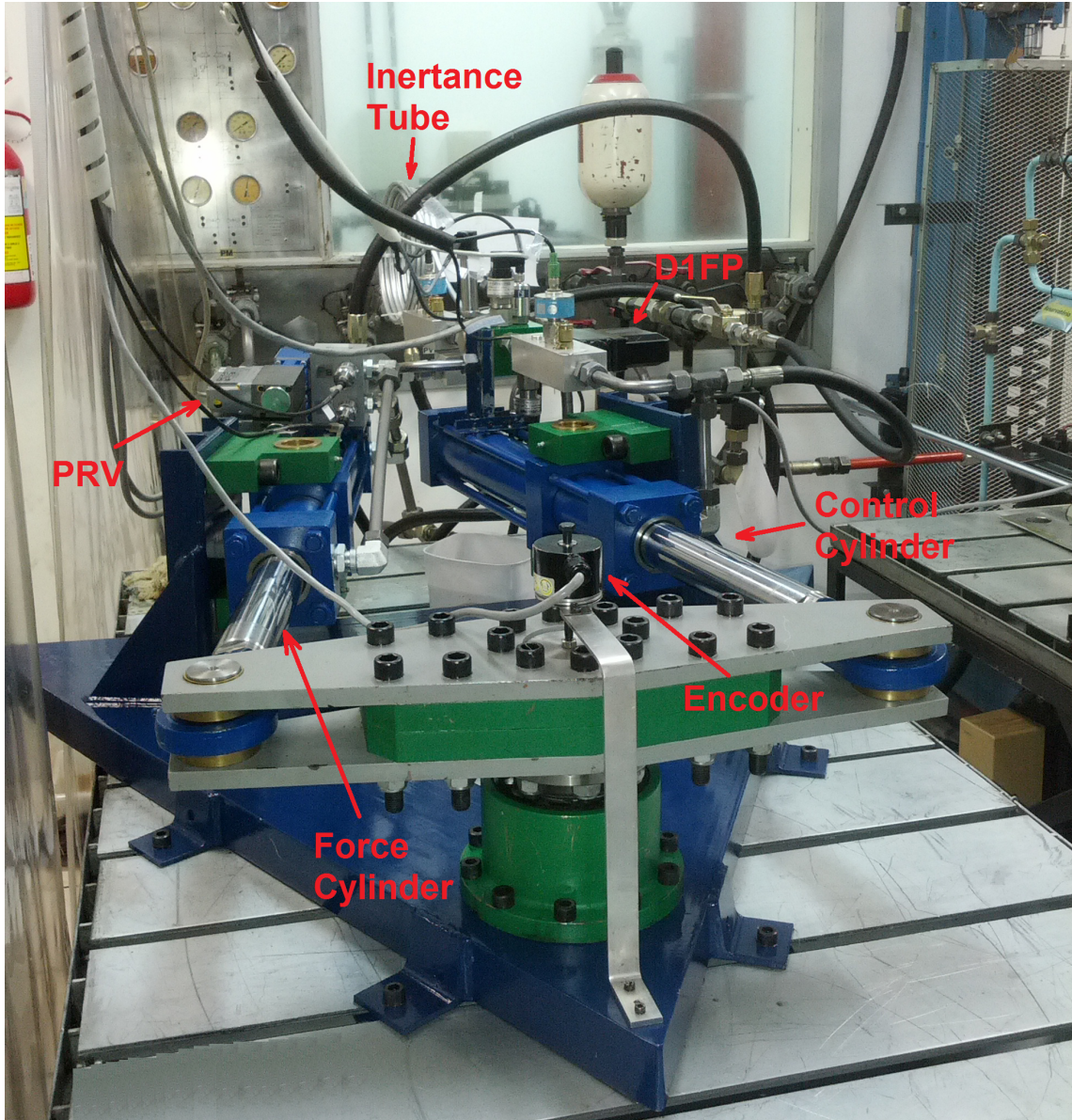


Figure 5.2: Hydraulic/mechanical system of the test bench

The “V” configuration has been developed with the intent of testing up to the angle variation of 90° , which is the condition applied for arresting the wind turbine (see section 2.4). The two pressure reduction valves (PRV), electronically commanded, regulate the pressure into the chambers of the force cylinder acting an accurate control in order to produce the desired force F_p .

The dynamical and geometrical features of the bench are here presented:

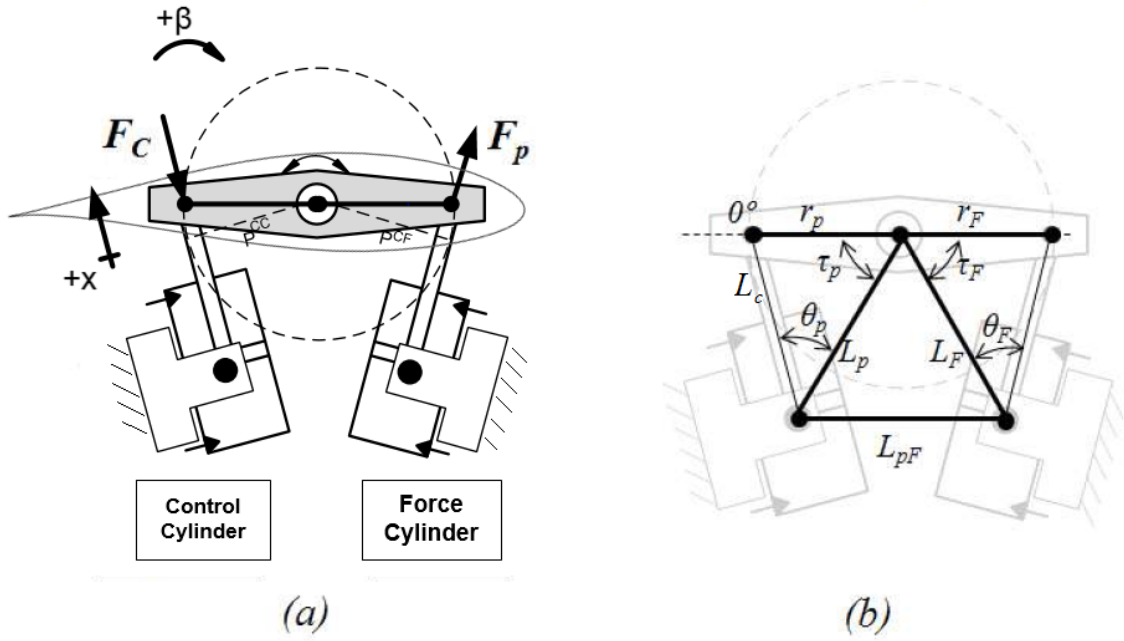


Figure 5.3: a) Scheme of the test bench b) Geometrical parameters [14]

The applied force F_p represents the action of the wind on the blade, which is highly and rapidly variable. However, in the tests those proprieties have been neglected considering the applied force constant or following low-frequency waves, since the objective of this study is to evaluate the performances of the control system rather than the acting forces, which have been widely discussed by Facundo [14].

When the pitch angle (β) is equal to 0, the blade is in the central position as shown in figure 5.3. The parameters L_p, L_F, L_{pF}, r_p and r_F evidenced in figure 5.3 b) are constant and summarized, along with known values of the angles τ_p and τ_F when $\beta = 0$, in the following table

Parameter	Value	Measure Unit
τ_p	73,98	[°]
τ_F	73,37	[°]
L_p	0,641	[m]
L_F	0,643	[m]
L_{pF}	0,361	[m]
r_p	0,3	[m]
r_F	0,3	[m]

Table 5.1: Geometrical Parameters [14]

Figure 5.3b) and table 5.1 defines the initial configuration of the mechanism which permits to investigate the way the force generated by the force cylinder is transmitted to the other one. In particular, using the theorems regarding the sine and cosine, the moment arms of the forces F_p and F_c are noted:

$$P^{CC} = \frac{L_p r_p \text{sen}(\tau_p + \beta)}{\sqrt{L_p^2 + r_p^2 - 2L_p r_p \text{cos}(\tau_p + \beta)}} \quad (5.1)$$

$$P^{CF} = \frac{L_F r_F \text{sen}(\tau_F + \beta)}{\sqrt{L_F^2 + r_F^2 - 2L_F r_F \text{cos}(\tau_F + \beta)}} \quad (5.2)$$

now inserting the data from table 5.1 into the above equations evidences that P^{CC} and P^{CF} are almost the same. Thus, observing that the couple of forces generates an unique moment, the two forces are equal in magnitude and have opposite direction.

For this reason, the external load applied to the hydraulic system object of this study has to be considered as the real force emitted by the flanked system, just opposite in direction.

Moreover, the use of the geometrical parameters allows to determine a relation between the pitch angle β and the motion parameter x of the piston rod acting on the pitch control.

Observing that:

$$L_c = \sqrt{L_p^2 + r_p^2 - 2L_p r_p \text{cos}(\tau_p + \beta)} \quad (5.3)$$

and considering $x = 0$ when $\beta = 0$, the correlation between angle and cylinder motion is:

$$x = 5,115 \cdot \beta \quad (5.4)$$

The communication between test bench and the system control, necessary for commanding the valves and acquiring the responses of the tested system, has been

realized using a dSpace unit. In specific dSpace is a company which realizes devices for HIL simulations. Therefore, the dSPACE DS1103 PPC and the connector panel DS 1103 have been used for transmitting data from/to the test bench via the software ControlDesk by dSpace which interacts with *Simulink*.

The next figure shows the complete test bench

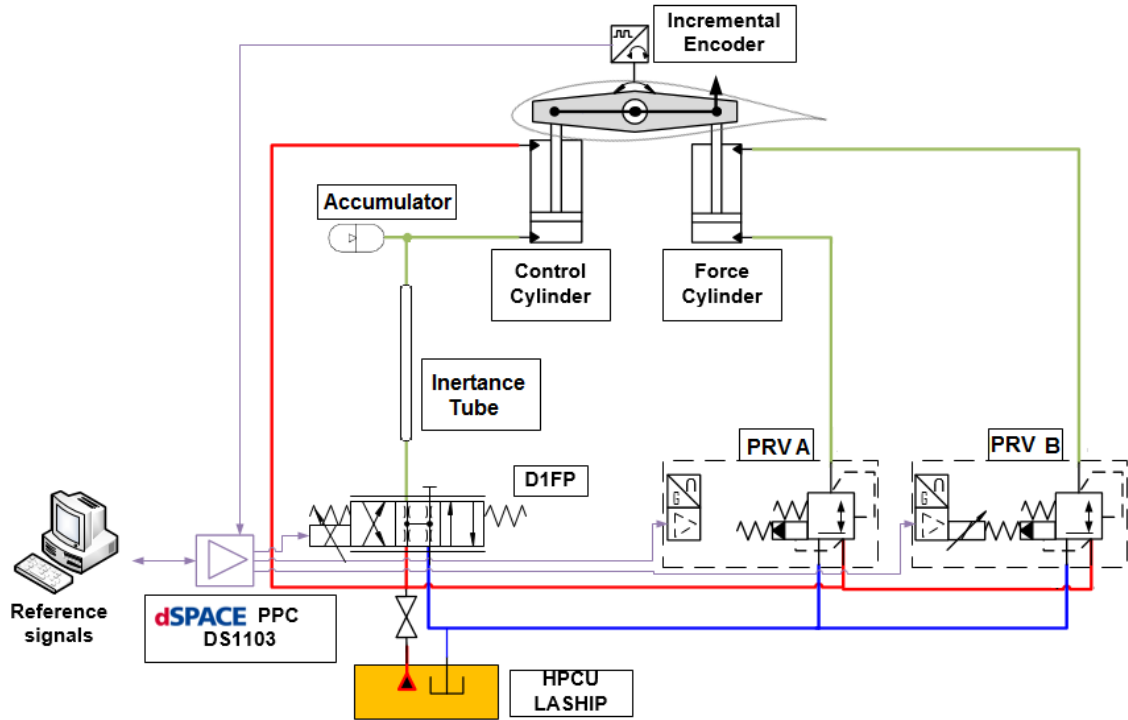


Figure 5.4: Test Bench Diagram (adapted from [14])

5.2 Simulations

Using the equation presented in chapter 4, the hydraulic system proposed in section 3.5 has been modelled in the software MATLAB/*Simulink*. The realized model is an accurate representation of the system shown in figure 3.8.

Simulink allows to test the model by performing dynamic simulations which can follow different configuration parameters, simulation time and inputs. In this study, simulations using the solver ode3 (Bogacki - Shampine) with fixed-step size of $1e-5$ have been performed for 40 seconds, in which step variations of either pitch angle or force F_c have been applied.

5.3 Results

Hereafter the results of both simulations and experiments are presented:

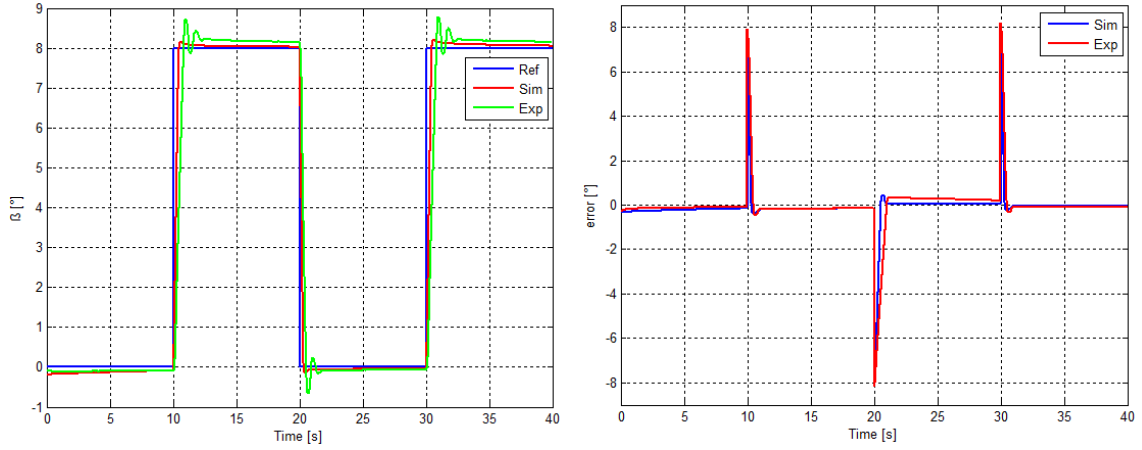


Figure 5.5: Responses of the system to angular steps using a force $F_c = 10$ kN

The parameters describing the above curves are reported in the next table:

Steps	t_r [ms]	t_s [ms]	M_p [%]	
0-8 [°]	414	599	1,8	Simulation
8-0 [°]	321	521	1,9	
0-8 [°]	776	1196	9,24	Experiment
8-0 [°]	534	927	8,43	

where

t_r is the rise time [ms]

t_s is the settling time [ms]

M_p is the maximum peak of the overshoot [%]

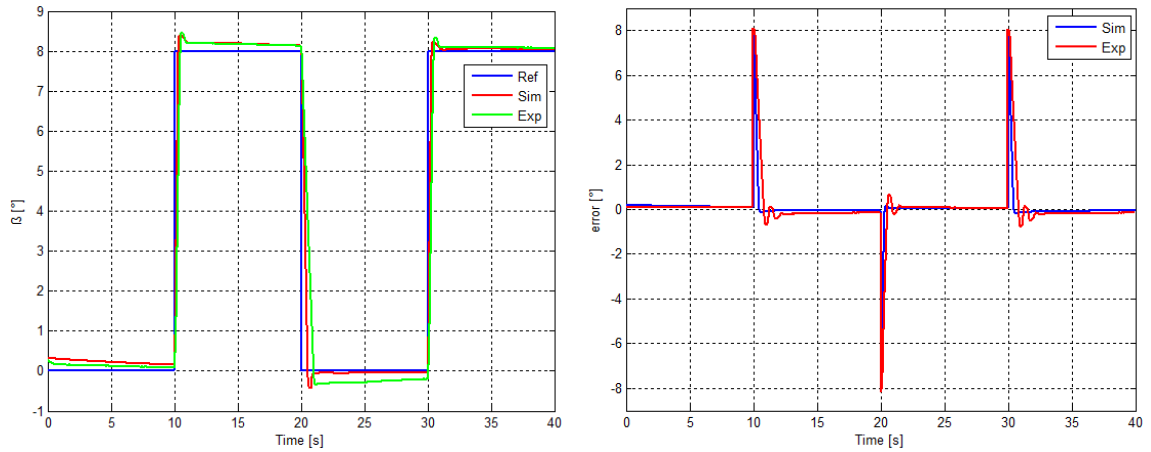


Figure 5.6: Responses of the system to angular steps using a force $F_c = -10$ kN

The parameters describing the above curves are reported in the table:

Steps	t_r [ms]	t_s [ms]	M_p [%]	
0-8 [°]	288	534	4,59	Simulation
8-0 [°]	545	685	5,28	
0-8 [°]	431	744	5,82	Experiment
8-0 [°]	1007	-	4,32	

The above diagrams show that the model replicates accurately the behaviour of the real system. They do not have the identical dynamic, the modelled system presents a smoother trend of the overshoot, but the differences are as expected and do not interfere with the purposes of the modelling. Hence, it is possible to conclude that a model which is an accurate representation of the real system has been developed. This permits to act on the model in order to evaluate the influences that parameter and system modifications may have on the response of the real system. Therefore, the model represents a very useful tool for assisting the analysis and optimization of the system.

For this reason the major part of the data shown now on have been obtained via simulations. The results shown in figure 5.6 and 5.7 have been achieved using a PI defined by the constants $K_p = 0.7$ and $K_i = 0.05$. Next several responses achieved using different PI controllers are compared:

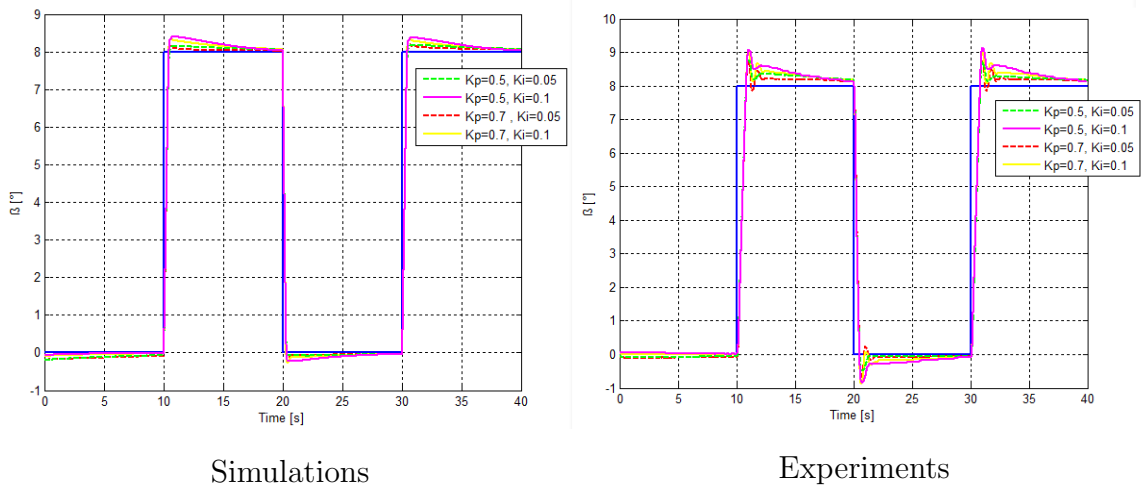


Figure 5.7: Responses of the system comparing different PI controllers

As it possible to notice the best performances, in term of tracking the reference, have been obtained using the lower integral constant $K_i = 0.05$ and the higher proportional effect $K_p = 0.7$. For this reason, those are the parameters used in all the simulations and tests presented up to now and henceforward.

Even though those values determine a response which satisfies the criteria of pitch system maximum speed equal to $19 \text{ }^\circ/\text{s}$ for 650 kW plants [39] which is the most critical condition found in the literature, the steady state value is reached with very slow dynamic. That is caused by the small entity of the integral parameter K_i . Increasing the integral constant improve the steady state conditions but rise the maximum value of the overshoot. The latter condition triggers an undesirable and critical phenomena of the valve. For describing it, the figures beneath have been introduced:

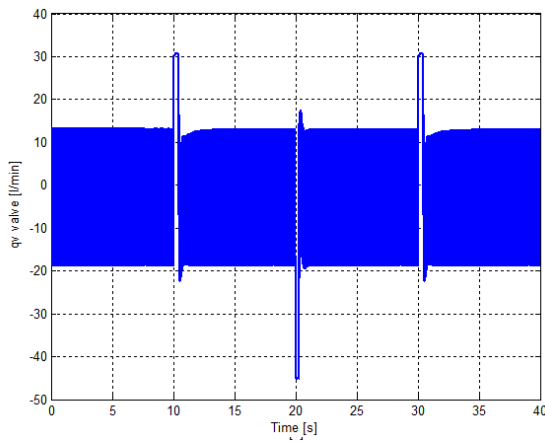


Figure 5.8: Flow rate through the valve

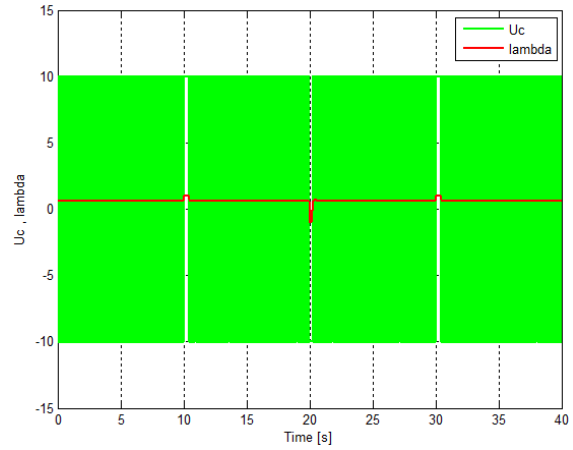


Figure 5.9: Control signals of the valve

Applied force $F_c = 10\text{kN}$

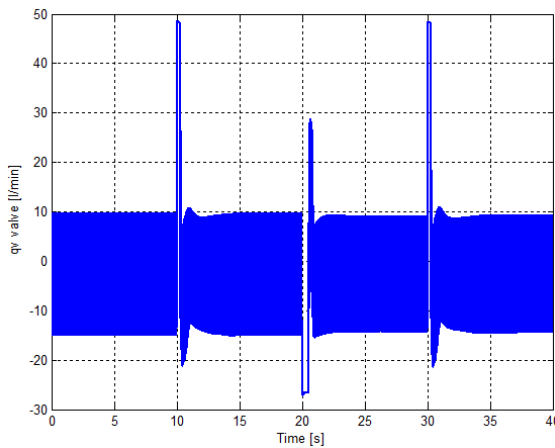


Figure 5.10: Flow rate through the valve

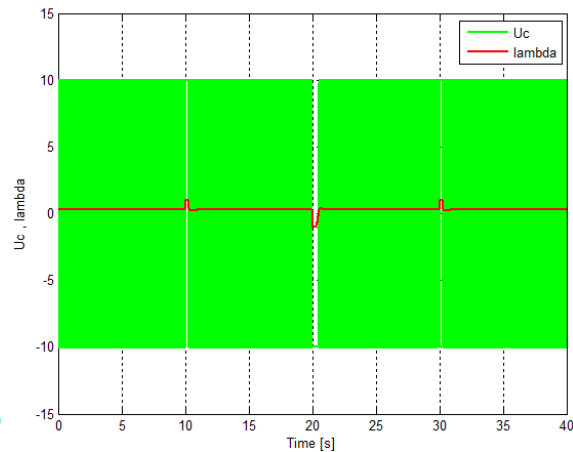


Figure 5.11: Control signals of the valve

Applied force $F_c = -10\text{kN}$

As can be seen the valve saturates; that is an unwanted phenomena for the SIHS since every instant at which the valve does not switch means energy leaks and efficiency reduction. Therefore, the considered value of K_p and K_i are the best compromise between dynamics of the steady state condition and saturation of the valve. For a better view a zoom of the saturation is proposed below

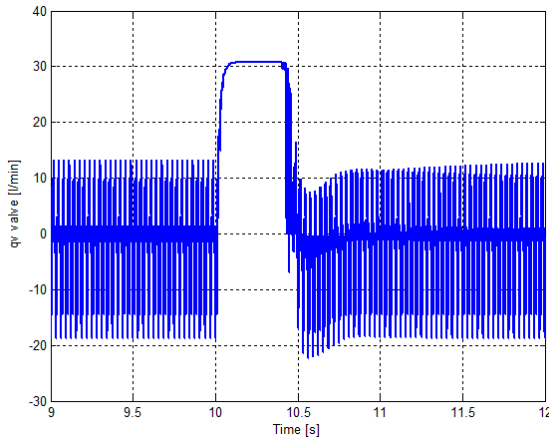


Figure 5.12: Enlargement of the flow rate through the valve

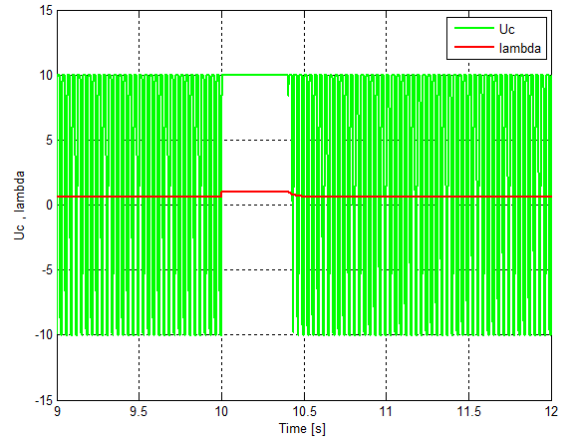


Figure 5.13: Enlargement of the control signals of the valve

Applied force to the system $F_c = 10\text{kN}$

The next graphs show the fluid pressure at different positions along the system. The pressure at the valve outlet oscillates cyclically within the range $p_{LP} - p_{HP}$ then at the end of the tube the accumulator damps the pulsation providing a pressure which is almost constant and identical to the load pressure of the cylinder; this accordingly with the SIHS functional principles (see section 3.3.1)

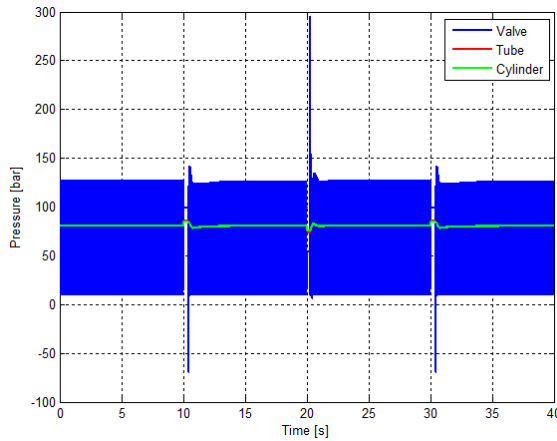


Figure 5.14: Pressures with $F_c = 10\text{kN}$

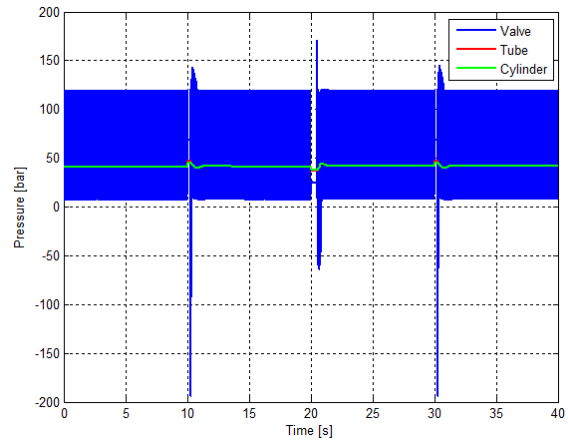


Figure 5.15: Pressures with $F_c = -10\text{kN}$

For a better view a zoom of the pressure peaks is proposed

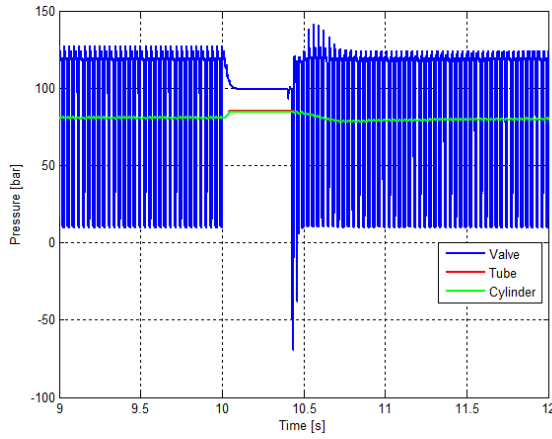


Figure 5.16: Enlargement of the pressures with $F_c = 10\text{kN}$

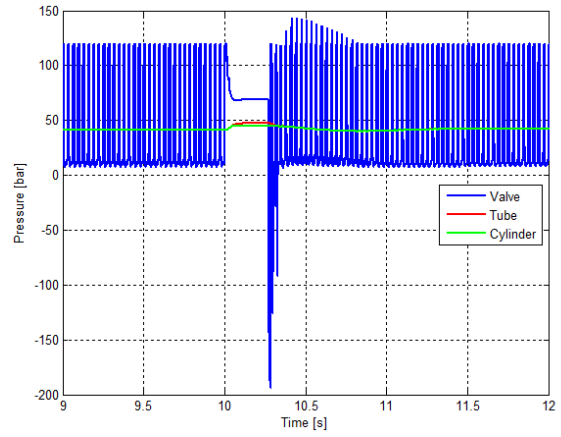
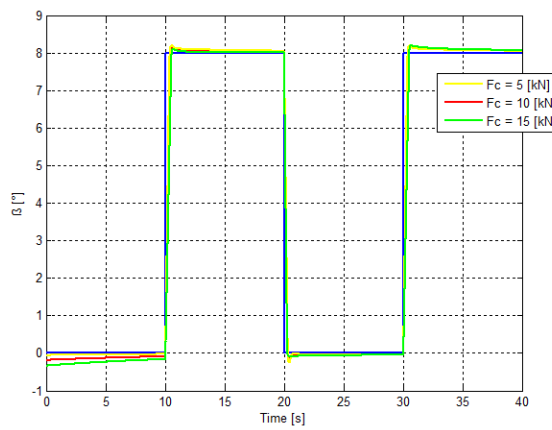
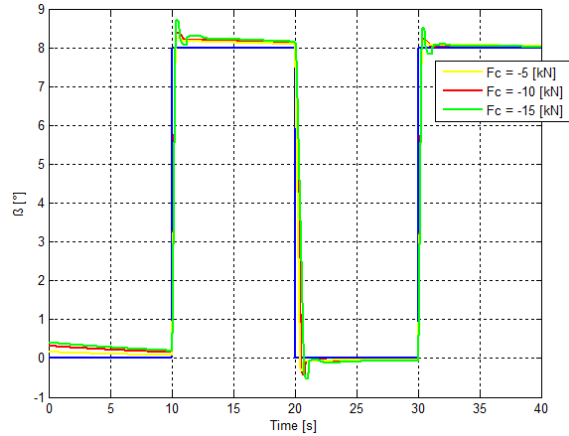


Figure 5.17: Enlargement of the pressures with $F_c = -10\text{kN}$

Next it has been demonstrated that the model is able to operate with different forces, both opposing and favoring the motion.



$F_c > 0$



$F_c < 0$

Figure 5.18: Simulated responses of the system comparing different forces

As expected the results achieved via experiments are comparable with the simulated ones.

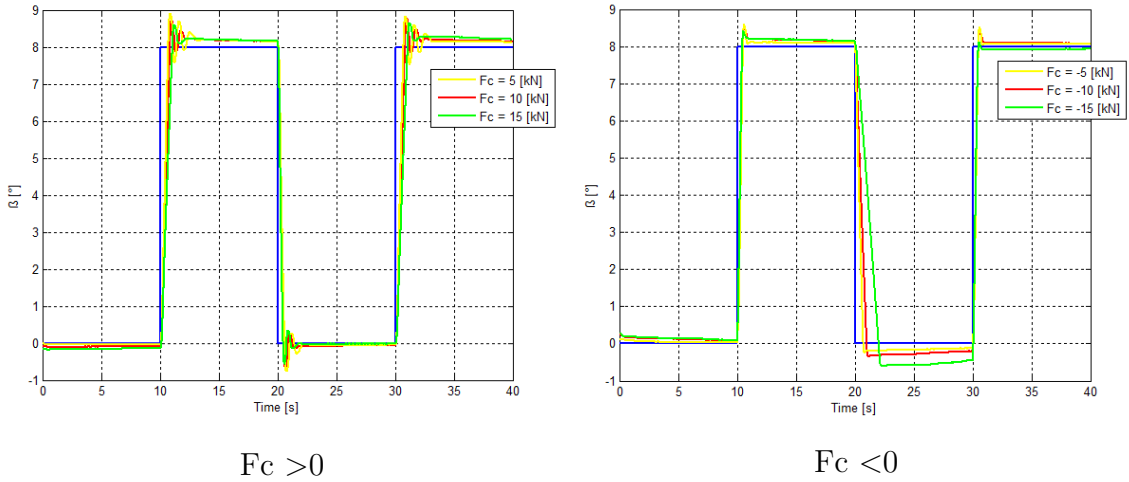


Figure 5.19: Experimental responses of the system comparing different forces

Theoretically, the system can operate up to a load force defined by the following equations:

$$\text{for } U_c = 10 \qquad U_c = -10:$$

$$F_c = P_{HP} \cdot A_A - P_{HP} \cdot A_B \qquad F_c = P_{LP} \cdot A_A - P_{HP} \cdot A_B \quad (5.5)$$

substituting the opportune values (see appendix B)

$$F_c = 29544 \text{ N} \qquad F_c = -25742 \text{ N}$$

However, leakage and friction phenomena have not been introduced in the equations 5.5. As a result, the above maximum and minimum values of the ideal force has to be reduced to a certain amount which is not easy to determine. For this reason, the limits of the real practicable force have been estimated by simulations. Observing the responses obtained, it has been noticed that the system is not able to accurately regulate the pitch angle using forces greater than 23 kN and lower than -13 kN.

Underneath the responses achieved via simulation of the system applying those values to the force F_c are shown

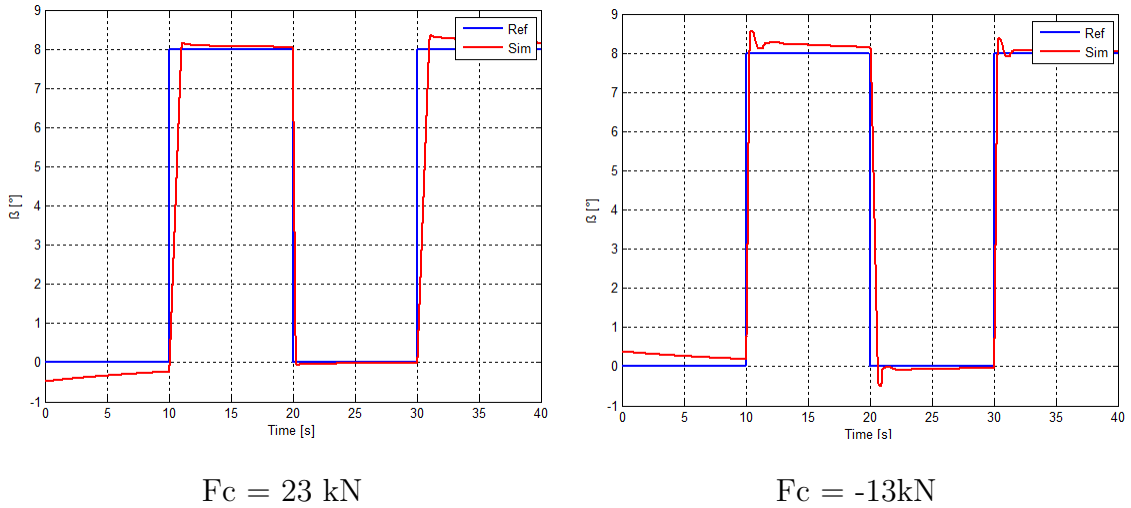


Figure 5.20: Responses using critical forces

In order to respect the integrability of the bench tests submitted to those extreme conditions have been avoided.

5.4 Energy Assessment

One of the objective of this work is establish whether the new system proposed gives advantages compared to the applications presently used for pitch control on wind turbine. To analyse the matter an energy assessment has been conducted.

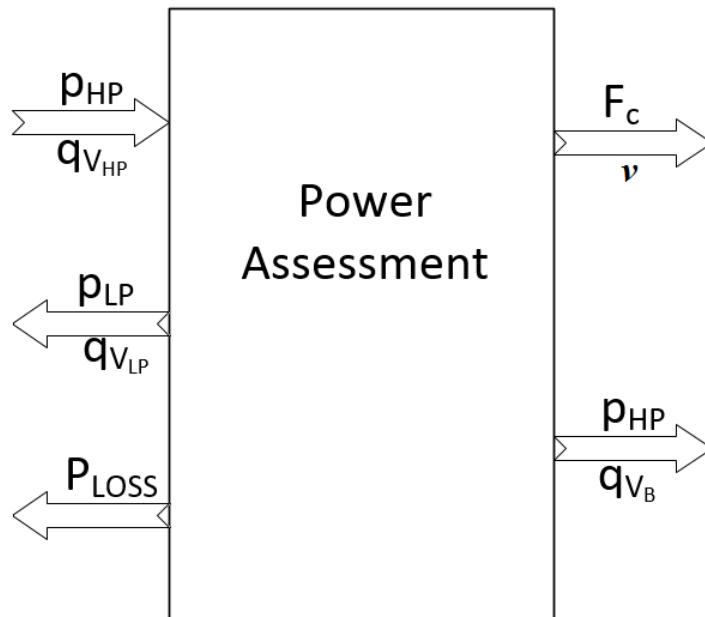


Figure 5.21: Diagram of the power assessment

The diagram shows the flows of energy towards and outwards the system. In particular they are expressed in form of power which is the instant rate of change over time of the energy. For calculating the power, it is possible to use hydraulic and mechanical relations which lead to:

$$\begin{aligned}
 P_{HP} &= q_{V_{HP}} \cdot p_{HP} \\
 P_{LP} &= q_{V_{LP}} \cdot p_{LP} \\
 P_B &= q_{V_B} \cdot p_{HP} \\
 P_{mec} &= \vec{F}_c \times \vec{v}
 \end{aligned}
 \tag{5.6}$$

where

P_{HP}	is the instant power present at the high pressure port of the power unit [W]
P_{LP}	is the instant power present at the low pressure port of the power unit [W]
P_B	is the instant power present at the port B of the cylinder [W]
P_{mecc}	is the useful power [W]
$q_{V_{HP}}, q_{V_{LP}}$ and q_{V_B}	are respectively the flow rates occurring at the high pressure port, low pressure port and port B of the cylinder [l/min]

Notice that, since the power and energy are scalar physical quantities the directions shown in diagram 5.21 are purely indicating a notation convention, which guides the attribution of the positive or negative sign to the scalar value. For each element, the variation of sign agrees with flow rates sense or the vector directions for the mechanical power.

The set of equations 5.6 does not include the hydraulic power lost along the system (P_{LOSS}) and not converted into the useful power P_{mecc} . However, the node analysis defines P_{LOSS} as:

$$\begin{aligned}
 P_{LOSS} &= P_{Hyd} - P_{mecc} \\
 &= P_{HP} - P_{LP} - P_B - P_{mecc}
 \end{aligned}
 \tag{5.7}$$

Since the useful power depends on the entity of the force F_c , it is interesting to study the power capacity of the system which is obtained applying the extreme conditions of the load force. Taking as reference the step response from 0° to 8° , the assessment has been conducted.

An equal assessment has been conducted on a system which represents the hydraulic systems currently present on wind turbines for pitch control. For modelling that system the SIHS considered up to now has been modified removing the inertance tube and the accumulator; in addition the control unit has been modified in order to using a control signal U_c proportional to the signal error $e(t)$ rather than a PWM. The *Simulink* diagram of the described system can be seen in figure 5.22

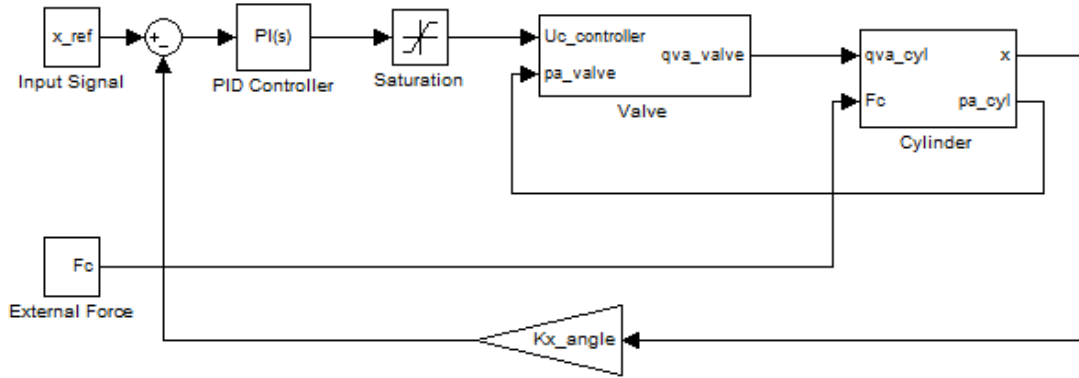


Figure 5.22: Simulink of the proportional system

That system presented the same problem related to the saturation of the valve. The assessment has been conducted using a PI controller characterized by $K_p = 2$ and $K_i = 0.05$ and the same conditions of the load force F_c .

It evidenced that even though both the systems have low efficiency, the SIHS demonstrates some advantages in term of energy savings. The results indicated a difference between the efficiencies of about 6 %.

6

Conclusions

This thesis presented an innovative hydraulic system for regulating the blade pitch angle of horizontal axis wind turbines.

After a brief overview the wind power and the digital fluid power state of art, the switched inertance hydraulic system (SIHS) proposed as object of this study was described.

Furthermore, the analytical models of the elements which compose the SIHS were defined and their implementation in the software *Simulink* presented. It resulted in obtaining a model which is an accurate representation of the whole hydraulic system.

The model was finally validated, by comparison with experimental results and the data achieved were reported.

To conclude, thanks to the energy assessment, was demonstrated that the SIHS proposed gives advantages in term of energy saving and higher efficiency than the systems currently used in wind industry for the considered application.

According to Linjama [8] one of the most critical problems which limits the application of digital hydraulics and in particular of the switching technology is the unavailability of commercial valves able to perform the specific requirements of the system. That has been noticed widely during the development of this work, since the valve in the presented application saturates frequently due to the flow demand by the cylinder. Although the D1FP valve chosen for the application has the best rate in commerce between high nominal flow rate and short time response, it does not satisfy the system requirements then it generates leakages which highly influence

the system efficiency. As pure matter of analysis, simulations performed using a modified SIHS substituting the D1FP valve with an ideal valve which has the same frequency response but higher nominal flow rate, resulted in improvements of the valve response and system efficiency.

Observing the graphs which show the pressure of the fluid, it can be noticed that cavitation phenomena occurred at the valve outlet. Since the graphs were obtained via software modelling rather than real experiments, the visible negative pressure peaks might be not caused by cavitation but be instead the manifestation of algebraic errors occurred during the simulations. However, this is a signal of criticalness of the system then it has to be analysed. The first approach in order to improve the pressure trend has been applying to the system a tube characterized by high flexibility which behaves as a capacitance and has the ability, according to Pérez [40], to modify the effective bulk modulus acting on the system. The data obtained by the simulations including the described tube showed that it smooths the pressure peaks within plausible values, however it also reduced the performances of the system. The results were promising but unfortunately, due to the complexity of the problem and the short available time the analysis of the cavitation phenomena has been abandoned. Nevertheless, the problematic has great relevance on the system and its analysis may represents a possible topic for future studies which may prosecute the author's attempt.

Other possible future developments feasible on the actual system in order to improve its accuracy and performances are

- implement the model *Simulink* realized by Facundo [14] resulting in consider the force F_c as a function of wind parameters
- optimize the controller using the well-known techniques for tuning the PID which however operate on linear systems, thus the linearisation of the actual system is requested
- simulate and test the arrest condition of the turbine ($\beta = 90^\circ$)

In addition, based on the discussion presented in section 3.5 potential next studies may regard the application of the SIHS to other control system.

Concluding, this thesis demonstrates that the SIHS has the potential to rise the efficiency of pitch control systems applied on wind turbines. Moreover, it pointed out that is just matter of using more opportune valves for improving the performances and efficiency of the SIHS itself. For these reasons the SIHS has to be considered has one of the most promising hydraulic system for pitch control in the next future.

References

- [1] <http://www.3tier.com>.
- [2] Global Wind Energy Council (GWEC), “Global wind statistics 2014,” February 2015.
- [3] Burton T., Sharpe D., Jenkins N., and Bossanyi E., *Wind Energy Handbook*. West Sussex, England: John Wiley & Sons, 2001.
- [4] Wagner H.J., “Introduction to wind energy systems,” *EPJ Web of Conferences*, vol. 54, 2013.
- [5] Manwell J.F., Mcgowan J.G., and Rogers A.L., *Wind Energy Explained*. USA: John Wiley & Sons, 2 ed., 2009.
- [6] Hau E., *Wind Turbines: Fundamentals, Technologies, Application, Economics*. Munich, Germany: Springer Heidelberg, 3 ed., 2013.
- [7] <http://www.boschrexroth.com>.
- [8] Linjama M., “Digital fluid power - state of the art,” *The Twelfth Scandinavian International Conference on Fluid Power*, May 2011.
- [9] Machado C., “Compensação de atrito em atuadores hidráulicos utilizando redes neurais,” 2003.
- [10] Furst F.L. and De Negri V.J., “Projeto de sistema hidráulicos de controle de posição.” Apostille, Florianópolis, 2002.
- [11] Pan M., Johnston D.N., Plummer A.R., Kudzma S., and Hillis A.J., “Theoretical and experimental studies of a switched inertance hydraulic system including

- switching transition dynamics, non-linearity and leakage,” *Journal of Systems and Control Engineering*, vol. 228, pp. 12–25, 2014.
- [12] Hydac Hydraulic Dampers Catalogue, 2014.
- [13] Rabie M.G., *Fluid Power Engineering*. Cairo, Egypt: McGraw-Hill Professional Publishing, 1 ed., 2009.
- [14] Facundo E.G., “Estudo das forças atuantes em mecanismos de regulação de ângulo de passo e desenvolvimento de um sistema emulador de cargas,” Master’s thesis, Universidade Federal de Santa Catarina, Florianópolis, 2012.
- [15] Johnston D.N., “The transmission line method for modelling laminar flow of liquid in pipelines,” *Proceedings of the Institution of Mechanical Engineers, Part I: Journal of Systems and Control Engineering*, pp. 1–12, 2012.
- [16] World Wind Energy Association (WWEA), “World wind resource assessment report,” December 2014.
- [17] Fthenakisa V. and Kimb H.C., “Land use and electricity generation: A life-cycle analysis,” *Renewable and Sustainable Energy Reviews*, vol. 13, pp. 1465–1474, 2009.
- [18] Marvel K., Kravitz B., and Caldeira K., “Geophysical limits to global wind power,” *Nature Climate Change*, vol. 322, no. 10, pp. 118–121, 2013.
- [19] <https://www.cia.gov/library/publications/the-world-fact-book/rankorder/2236rank.html>.
- [20] Archer C. K. and Caldeira K., “Global assessment of high altitude wind power,” *Energies*, vol. 2, pp. 307–319, 2009.
- [21] Xi L., McElroy M.B., and Kiviluoma J., “Global potential for windgenerated electricity,” *Proceedings of the National Academy of Sciences of the United States of America*, vol. 106, pp. 10933–10938, 2009.
- [22] Rickenberg F., “Valve. us patent no. 1757059,” 1930.
- [23] Murphy R. and W. J., “Hydraulic control system. us patent no. 3038449,” 1962.

- [24] Ballard R. L., “System for minimizing skidding. us patent no 3528708,” 1968.
- [25] Johnston D.N., “A switched inertance device for efficient control of pressure and flow,” *Bath/ASME Fluid Power and Motion Control Symposium*, pp. 1–8, 2009.
- [26] Manhartsgruber B., Mikota G., and Scheidl R., “Modelling of a switching control hydraulic system,” *Mathematical and Computer Modelling of Dynamical Systems*, pp. 329–344, 2005.
- [27] Kogler H. and Scheidl R., “Two basic concepts of hydraulic switching converters,” *Proceedings of the First Workshop on Digital Fluid Power*, pp. 113–128, 2008.
- [28] Hettrich H., Bauer F., and Fuchshumer F., “Speed controlled, energy efficient fan drive within a constant pressure system,” *Proceedings of the Second Workshop on Digital Fluid Power*, pp. 62–71, 2009.
- [29] De Negri V.J., Wang P., Plummer A., and Johnston D. N., “Behavioural prediction of hydraulic step-up switching converters,” *International Journal of Fluid Power*, 2013.
- [30] Brown F.T., “Switched reactance hydraulics: a new way to control fluid power,” *Proc. National Conference on Fluid Power*, pp. 25–34, 1987.
- [31] Plckinger A., Scheidl R., and Winkler B., “Performance, durability and applications of a fast switching valve,” *Proceedings of the Second Workshop on Digital Fluid Power*, pp. 129–143, November 2009.
- [32] Gomes S.C.P., “Modelagem de atritos internos às articulações de robôs manipuladores,” *XIII Congresso Brasileiro de Engenharia Mecânica*, 1995.
- [33] Linsingen I.V., *Fundamentos de Sistemas Hidráulicos*. Florianopolis, SC: Editora da UFSC, 2 ed., 2003.
- [34] Merritt H.E., *Hydraulic Control Systems*. New York, USA: John Wiley & Sons, 1 ed., 1967.

- [35] Krus P., Weddfelt K., and Palmberg J.-O., “Fast pipeline models for simulation of hydraulic systems,” *Journal of Dynamic Systems, Measurement, and Control*, vol. 116, pp. 132–136, 1994.
- [36] Johnston D. N., “An enhanced transmission line method for modelling laminar flow of liquid in pipelines,” *Proceedings of the Institution of Mechanical Engineers, Part I: Journal of Systems and Control Engineering*, 2013.
- [37] De Negri V.J., Nostrani M.P., Wang P., Johnston D.N., and Plummer A., “Modelling and analysis of hydraulic step-down switching converters,” *International Journal of Fluid Power*, 2015.
- [38] Nostrani M.P., “Estudo teórico-experimental de um posicionador utilizando hidráulica digital para aplicação em turbinas eólicas,” Master’s thesis, Universidade Federal de Santa Catarina, Florianópolis, 2015.
- [39] Fingerish L. and J. K., “Controls advanced research turbine (cart) commissioning and baseline data collection,” *Technical Report*, October 2002.
- [40] Pérez J.A.L., “Controle robusto de força em atuadores hidráulicos aplicando a teoria de realimentação quantitativa,” 2012.
- [41] Goodson R.E. and L. R.G., “A survey of modeling techniques for fluid line transients,” *Journal Basic Engineering*, vol. 94, p. 474482, 1972.
- [42] Stecki J.S. and D. D.C., “Fluid transmission lines distributed parameter models. part 1: a review of the state of the art,” *Proc IMechE, Part B: Journal Engineering Manufacture*, pp. 215–228, 1986.
- [43] Johnston D. N., “Efficient methods for numerical modeling of laminar friction in fluid lines,” *Journal Dynamic System Measure Control*, vol. 128(4), pp. 829–834, 2006.
- [44] Trikha A.K., “An efficient method for simulating frequency-dependent friction in transient liquid flow,” *Journal Fluids Engineering*, vol. 97, pp. 97–105, 1975.
- [45] <http://people.bath.ac.uk/ensdnj/models>.

Appendix A

Transmission Line Method (TLM)

Several techniques are available from modelling time-varying flow and pressure in fluid pipelines. Typically in hydraulic systems the short length of the pipelines make possible to neglect the dynamics of the flow, though it is fairly rapid. In those cases the pipe can be modelled simply using lumped parameters. On the other hand, in many other cases such as the use of long pipelines or applications where the valve initially open is demanded to suddenly close, the pipe model needs to consider the compressibility and inertia of the fluid. The method of characteristics (MOC) can be an extremely accurate method and can give results that are virtually indistinguishable from analytical solutions, however it requires more time and computational efforts than other methods such as the TLM. The transmission line method is a high efficiency technique for modelling pipelines, it demands about the 5 % of the computational time needed by the MOC and gives the possibility to determine useful parameters such as the transients of pressure or viscosity friction.

It makes use of the inherent delay in transmission of pressure and flow from one end of the line to the other. In the TLM, the line is not subdivided, but pressure and flow (or other variables) at each end are stored for a number of time steps. The variables (pressure and flow, or equivalent) at a new time step are calculated from the variables at the other end delayed by a period of time [15].

A pipeline can be represented by figure A.1 and the transmission matrix [41] given by A.1

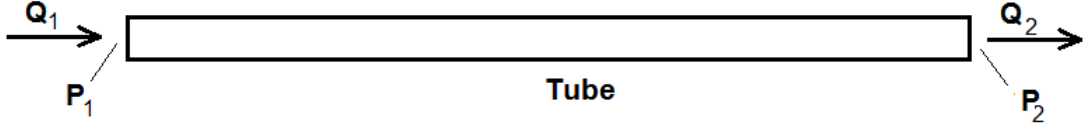


Figure A.1: Pipeline

$$\begin{pmatrix} Q_2 \\ P_2 \end{pmatrix} = \begin{pmatrix} \cosh Ts\sqrt{N} & -\frac{1}{Z_C\sqrt{N}}\sinh Ts\sqrt{N} \\ -Z_C\sqrt{N}\sinh Ts\sqrt{N} & \cosh Ts\sqrt{N} \end{pmatrix} \begin{pmatrix} Q_1 \\ P_1 \end{pmatrix} \quad (\text{A.1})$$

T is the time needed for a wave to pass along the line. It can be calculated as

$$T = \frac{L}{c} \quad (\text{A.2})$$

where c is the speed of sound in the line.

Z_C is the inviscid characteristic impedance of the line and it can be defined as

$$Z_C = \frac{\rho c}{A} \quad (\text{A.3})$$

where A is the cross area of the line.

The TLM is a method to approximate this equation in the time domain.

N is a frequency-dependent function that depends on the type of friction model that is used [42].

Introducing characteristic C_1 and C_2 such that

$$\begin{aligned} P_1 &= C_1 + Z_C Q_1 \\ P_2 &= C_2 + Z_C Q_2 \end{aligned} \quad (\text{A.4})$$

it can be obtained

$$\begin{aligned} C_1 &= e^{-Ts\sqrt{N}}(P_2 + Z_C\sqrt{N}Q_2) + Z_C(\sqrt{N} - 1)Q_1 \\ C_2 &= e^{-Ts\sqrt{N}}(P_1 + Z_C\sqrt{N}Q_1) + Z_C(\sqrt{N} - 1)Q_2 \end{aligned} \quad (\text{A.5})$$

The block diagram in figure A.2 is an exact representation of equation A.1.

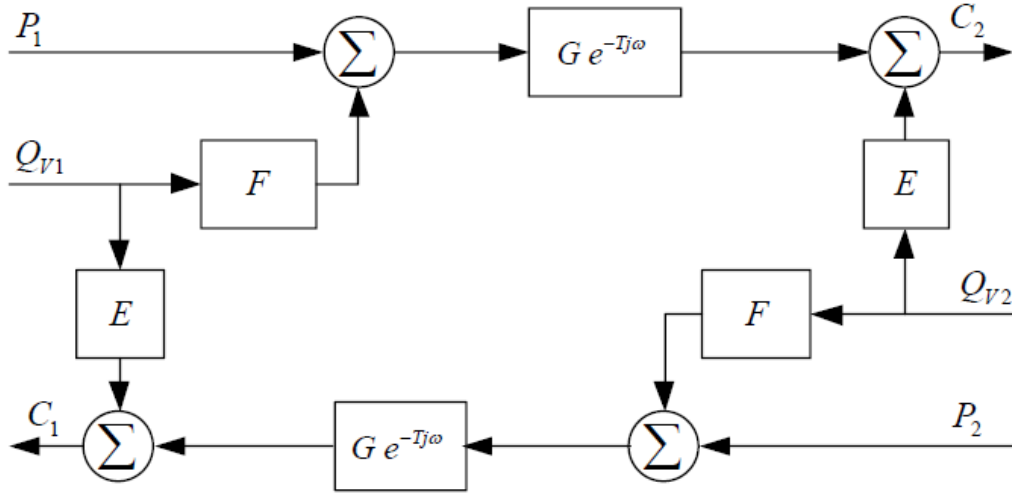


Figure A.2: Block diagram for the TLM [15]

If the terms are [35]:

$$E = Z_c(\sqrt{N} - 1) \quad (\text{A.6})$$

$$F = Z_c\sqrt{N} \quad (\text{A.7})$$

$$G = \exp^{-Tj\omega(\sqrt{N}-1)} = \exp^{-\beta j\alpha(\sqrt{N}-1)} \quad (\text{A.8})$$

where α is the non-dimensional frequency

$$\alpha = \frac{r^2\omega}{v} \quad (\text{A.9})$$

and β is the dissipation number

$$\beta = \frac{vL}{cr^2} = \frac{vT}{r^2} \quad (\text{A.10})$$

if quasi-steady laminar resistance is assumed, N is given by

$$N = 1 + \frac{8}{j\alpha} \quad (\text{A.11})$$

Including the effect of the velocity variation with the frequency [42] and assuming laminar flow but neglecting thermal effects, N is given by [15]

$$N = \frac{1}{1 - \frac{2J_1(z)}{zJ_0(z)}} \quad (\text{A.12})$$

where $z = j\sqrt{j\alpha}$

Krus [35] neglected unsteady friction and proposed simple transfer function which however are not good approximations to the exact terms, equation A.3 and A.4, and need an additional filter term in G to represent unsteady friction. Johnston [43] incorporated in the TLM a method developed by Trikha [44] for approximating unsteady laminar friction for used with MOC. Johnston defined a friction function H

$$H = \frac{j\alpha}{\frac{z J_0(z)}{2 J_1(z)} - 1} \quad (\text{A.13})$$

The TLM significantly underestimates the pressure rise for low β and overestimates for high β . This indicates that the TLM model produces an error in the effective capacitance of the pipeline. The error in the capacitance can be eliminated by adjusting the characteristic impedance using equation A.14 [15]. The model with this adjustment applied is the most accurate TLM approximation currently present in the literature and it is the model used for this thesis.

$$Z_C = \frac{\rho c}{A} \left(1 + \kappa [1 - \exp^{-4\beta}] + 2 \sum_{i=1}^k \frac{m_i}{n_i} - 4\beta \right) \quad (\text{A.14})$$

κ, m_i, n_i are empirical factors

Thanks to the Centre for Power Transmission and Motion Control of the University of Bath, the TLM models have been implemented in MATLAB/*Simulink* and are available for free downloading [45].

Appendix B

Component Details

Along the thesis the hydraulic components which compose the SIHS have been described. However, the characteristic parameters which define those elements are not fully introduced. This section lists the most significant between them.

Based on figure 3.8

Switching valve

Producer: Parker Hanninfin

Code: D1FPE50MA9NB01

Max. operating pressure: 350 bar

Nominal flow rate: 40 l/min at $\Delta p = 35$ bar

Flow maximum: 90 l/min (at $\Delta p=350$ bar)

Leakage at 100 bar: <400 ml/min

Step response at 100% step: <3.5ms

Hydraulic Cylinder

Producer: Bosch Rexroth

Code: CDT3MT4/80/56/500/Z/1X/B11HFDTWW

Maximum operating pressure: 210 bar

Piston diameter: 80 mm

Piston area (A_A): 50.26 cm^2

Ring area (A_B): 25.63 cm^2

Stroke length: 500 mm

Piston mass: 3.6 kg

Rod mass: 10.0 kg

Inertance Tube	Length: 6m Diameter: 7.1 mm
Accumulator	Producer: Hydac Nominal volume: 0.32 l Permitted oprating pressure: 300 bar Height : 120 mm Diameter: 96 mm Weight : 1.8 kg Maximum operating flow rate: 95 l/min

Based on the hydraulic circuit showed in figure 5.4, the components which compose the force emulator are next coded

Force Cylinder	Bosch CDT3MT4/80/56/500/Z/1X/B11HFDTWW
Pressure Reducing Valve A (PRV A)	Bosch DREBE6X-1X/175MG24K31A1M
Pressure Reducing Valve B (PRV B)	Bosch DREBE6X-1X/175MG24K31A1M
Incremental Encoder	Veeder Root B58N2048D8BA50

The oil used in both simulations and experiments is the mineral oil Mobil DTE 24 (ISO VG32). It has been considered characterized by effective bulk modulus $\beta_e = 1.4$ GPa, kinematic viscosity $\nu = 33.15$ cSt and density $\rho = 842$ kg/m³.

Furthermore, the pumps of the power unit have been set to the values $P_{HP} = 120$ bar and $P_{LP} = 10$ bar.

Appendix C

Matlab Code

```
% SIHS for pitch control - Parameters
```

```
clear all;  
clc;  
close all;
```

```
% Power Unit
```

```
p_HP = 120e5;  
p_LP = 10e5;
```

```
% Oil Mobil DTE 24 (ISO VG32)
```

```
Be = 1.4e9; % Bulk Modulus[Pa]  
visc = 33.15; % Viscosity[cSt]  
rho = 842; % Density[kg/m^3]
```

```
% D1FP valve parameters
```

```
Qn = 40; % Nominal Flow Rate[l/min]  
dp_n = 35e5; % [Pa]  
Un = 10;
```

```
Kv = Qn/(60e3*sqrt(dp_n)); % Flow Coefficient
```

```
Kvin = 0.4e-3/60/sqrt(2*100e5); % Leakage coefficient, 400 [ml/min] at 100 bar
```

```
% Valve Dynamics
```

```
wn=142.8*2*pi;
```

```

E=0.9;

% Cylinder

Aa = 50.26e-4;           % m^2
rA = 1.96;
Ab = Aa / rA;

x0_cyl = 405e-3         % [m]
Va_0 = Aa * x0_cyl;

Cin = 0;

M_piston = 3.6         % [kg]
M_rod = 10;
M_cyl = M_piston + M_rod;
M_ext = 0;
M_total = M_ext + M_cyl;

Kx = 0;

% Controller

Kx_angle = 1/5.115e-3;

Kp_controller = 0.7;
Ki_controller = 0.05;

freq_control = 32;

% Friction Force

polyp = [6.511e4 1.298e3 1.047e3 1.498e3];
polyn = [-7.6699e4 -3.049e3 -1.542e3];

Fsp=1.506e3;
Fsn=-1.527e3;
dxlimp=5.03e-3;
dxlimn=-5.985e-3;
dx0p=2.515e-4;
dx0n=-2.992e-4;

```


% Tube Parameters

```
L_tube = 6; % Length [m]
di_tube = 0.0071; % Diameter [m]
p_init_tube = 0e5; % Initial Pressure [bar]
q_init_tube = 0.1; % Initial Flow Rate [l/s]
nterms=4; % Factor numbers of the friction
```

% Accumulator

```
p0_acc = 50e5; % [Pa]
k = 1.4;
V0_acc = 0.32e-3; % m^3
```

```
A_int = pi*(9e-3)^2/4;
A_ext = pi*(12e-3)^2/4;
```

```
cd = 0.7;
```

```
A_acc = A_ext - A_int;
```

```
Kv_acc = cd*A_acc*sqrt(2/rho);
```